DOI: 10.26599/FSHW.2026.9250916

Contents lists available at SciOpen

Food Science and Human Wellness

journal homepage: https://www.sciopen.com/journal/2097-0765

China Food Publishing Co.

Corosolic acid alleviates NAFLD mice reduced by high-fat diet by regulating cGAS-STING pathway via the microbiota-gut-liver axis

Kaiwei Cai[a], Zihao Chen[a], Jingheng Chen[a], Jingtao Yu[a], Xingyuan Zhang[a], Deng Song[c], Yuguang Chi[a], Yanlong Chen[a], Zhiyong Xie[b], Pei Li[a,d,*], Qiongfeng Liao[a,*]

[a]*State Key Laboratory of Traditional Chinese Medicine Syndrome, School of Pharmaceutical Sciences, Guangzhou University of Chinese Medicine, Guangzhou, Guangdong, 510006, PR China.*

[b]*School of Pharmaceutical Sciences (Shenzhen), Sun Yat-sen University, Guangzhou, Guangdong, 510006, PR China*

[c]*Yuebei People's Hospital, Shaoguang, Guangdong, 512000, PR China*

[d]*Science and Technology Innovation Center, Guangzhou University of Chinese Medicine, Guangzhou, Guangdong Province, 510006, China*

ABSTRACT: Corosolic acid (CRA) is a bioactive compound commonly utilized as a functional ingredient in health food formulations. However, its effects on the pathophysiology of non-alcoholic fatty liver disease (NAFLD) and the associated gut microbiota have remained largely uninvestigated. The study demonstrated that CRA administration reduced fat accumulation, attenuated body weight gain, and normalized serum lipid levels in NAFLD mice in a dose-dependent manner. Mechanistically, CRA appeared to modulate the gut-liver axis by enriching the growth of beneficial, short-chain fatty acids (SCFAs)-producing beneficial gut microbiota (e.g., *Bacteroides*, *Prevotellaceae_UCG-001*) while concurrently suppressing harmful bacteria implicated in liver pathology (*Lachnoclostridium*, *Ileibacterium*, *Colidextribacter*). Additionally, CRA enhanced the production of SCFAs in both gut contents and liver tissue. Transcriptomic analysis further elucidated CRA's anti-inflammatory role, revealing its capacity to suppress inflammation by regulating pyroptosis and downregulating IL-1β expression. Moreover, these anti-inflammatory effects were attributed to the modulation of the cGAS-STING pathway and subsequent reduction in NLRP3 and IL-1β expression, ultimately leading to alleviation of liver inflammation. Collectively, these findings highlight CRA's potential as a dietary supplement for NAFLD prevention and management.

Keywords: Corosolic acid; non-alcoholic fatty liver disease; gut microbiota; short-chain fatty acids; pyrodeath; cGAS-STING

1. Introduction

Non-alcoholic fatty liver disease (NAFLD) has become a widespread chronic liver condition globally, impacting over 30% of the population[1]. NAFLD includes a range of liver disorders from simple steatosis to non-alcoholic steatohepatitis, which can progress to liver fibrosis, cirrhosis, and hepatocellular carcinoma[2]. As NAFLD is increasingly associated with metabolic syndrome, obesity, and type 2 diabetes, recent research has also highlighted the role of the gut microbiota in its pathogenesis[3].

***Corresponding author**
lipei@gzucm.edu.cn, zyfxliao@gzucm.edu.cn

Received 20 June 2025
Received in revised from 20 August 2025
Accepted 10 September 2025

The gut microbiota is essential for maintaining metabolic and immunological balance[4, 5]. An imbalance or dysbiosis in makeup of gut microbiota and function has been commonly observed in individuals with NAFLD, indicating a potential correlation between gut microbial composition and liver health[6]. Prior research has demonstrated that enhancing the prevalence of serotonin-associated gut microbiota, including Bacteroides and Parabacteroides, can alleviate NAFLD and obesity[1]. Specifically, the intestinal flora is capable of generating diverse metabolites, such as short-chain fatty acids (SCFAs), mainly resulting from the fermentation of dietary fibers by particular types of bacteria[7]. For instance, reduced levels of butyrate-producing *Bifidobacterium* in NAFLD patients may improve intestinal barrier function, reducing translocation of bacterial endotoxins by the gut-liver axis and promoting liver inflammation and steatosis[8]. Therefore, comprehending the interaction between gut microbiota composition, SCFAs production, and hepatic metabolism offers novel insights into the pathophysiology of NAFLD. Targeting the gut microbiota by dietary treatments, prebiotics, probiotics, or fecal microbiota transplantation (FMT) has therefore been proposed as a potential therapeutic approach for NAFLD[9]. Future research is necessary to elucidate the mechanistic links between specific microbial species, SCFAs profiles, and NAFLD progression, as well as to identify therapeutic strategies that favorably modulate gut microbiota to mitigate NAFLD.

The cGAS-STING pathway is essential in the pathogenesis of NAFLD, as it triggers inflammatory responses that exacerbate liver injury. Specifically, the activation of cGAS-STING facilitates the release of IL-1β and enhances the expression of NLRP3, resulting in inflammasome activation and subsequent pyroptosis mediated by GSDMD[10]. Furthermore, SCFAs enhance intracellular Calcium (Ca^{2+}) levels and facilitate MAVS-dependent mtDNA release, thereby activating the cGAS-STING-IFN-I axis by stimulating GPR43 signaling in macrophages[11], potentially modulating inflammatory responses and providing protective effects against NAFLD. Collectively, these elements form a complex network of interactions, emphasizing the cGAS-STING pathway as a pivotal element in the pathophysiology of NAFLD.

Corosolic acid (CRA), a natural chemical found in *Crataegus pinnatifida Bunge* (Shan Zha or hawthorn), has received considerable attention in recent research for its potential therapeutic effects in liver diseases, particularly NAFLD. C*rataegus pinnatifida Bunge* is a widely consumed functional food, and it's often promoted as a nutritional supplement due to its health-promoting properties[12, 13]. Research has confirmed that the hepatoprotective effects of *Crataegus pinnatifida Bunge* in NAFLD are primarily mediated through the modulation of the intestinal flora and its metabolic products, SCFAs[14, 15]. Consequently, CRA appears to foster the proliferation of advantageous bacterial species, therefore increasing the synthesis of SCFAs, which may contribute to metabolic homeostasis and exert hepatoprotective anti-inflammatory effects. Consistent with this, CRA has anti-inflammatory effects in NAFLD mice by reducing pro-inflammatory cytokines (interleukin-1 beta and interleukin-6) via regulation of the AMPK pathway in the liver[13]. Moreover, CRA influences liver metabolism by modulating lipid profiles, insulin sensitivity, and inflammatory responses, all of which are essential determinants in the advancement of NAFLD[16]. Given its dual role as a dietary supplement and a potential gut microbiota regulator, CRA presents a compelling candidate for NAFLD

management. Further investigation into the effects of CRA on SCFAs profiles and their subsequent impact on liver health may reveal novel avenues for dietary interventions targeting NAFLD.

This study investigated the impact of CRA on NAFLD, delving into the associated mechanisms concerning intestinal microecology, particularly changes in gut microbiota and SCFAs. Specifically, CRA augments the synthesis of SCFAs, these SCFAs, in turn, can regulate the cGAS-STING pathway, thereby contributing to the amelioration of NAFLD. These findings provide a theoretical basis for the potential application of CRA as a dietary supplement or as a candidate for therapeutic drug development in the management of NAFLD and potentially related metabolic conditions such as obesity.

2. Materials and methods

2.1 Materials

CRA was obtained from the Biopurify Co., Ltd. (Sichuan, China). High-fat feed was provided by Research Diets Inc (NJ, USA). Tribromoethanol purchased from Nanjing Aibei Biotechnology Co., Ltd. (Nanjing, China). Triglyceride (TG), total cholesterol (TC), aspartate aminotransferase (AST) and alanine aminotransferase (ALT), high-density lipoprotein cholesterol (HDL-C), low-density lipoprotein cholesterol (LDL-C) were provided by the Jiancheng Bioengineering Institute (Nanjing, China). Glucometer was purchased from Yuwell (Jiangsu, China). TRIzol reagent, ChamQ SYBR qPCR Master Mix, Hiscript III RT SuperMix for RT-PCR and BCA Protein Assay Kit were obtained from CWBIO (Beijing, China). The primers were synthesized by Sangon (Shanghai, China). The GAPDH antibody was obtained from Abcam (MA, USA). NLRP3, p-STING, GSDMD and IL-1β antibodies were obtained from Cell Signaling Technology (MA, USA). cGAS, STING, and GSDMD provided by Immunoway (Beijing, China). Goat anti-rabbit IgG secondary antibody was obtained from Affinity (TX, USA). Rapid sealing fluid was obtained from Vogi Biotechnology Co. Ltd. (Shanghai, China). Acetic acid, propionic acid, isobutyric acid, butyric acid, pentanoic acid, the purity of SCFAs above was more than 98% provided by Sigma-Aldrich (MO, USA). Vadimezan (DMXAA) was provided by MedChemExpress (MCE, USA).

2.2 Animal treatment and sample collection

Male C57BL/6J mice (8 weeks old) were obtained from the Guangdong Medical Laboratory Animal Center (Foshan, China; SCXK 2022-0002). Prior to the experimental procedures, mice were acclimatized for one week under standard conditions. Subsequently, the animals were allocated at random to two groups: a control group (Control, $n = 10$) and an NAFLD model group (Model, $n = 40$). To induce NAFLD, mice in the Model group were fed a high-fat diet (HFD) containing 60 kcal% fat, while the Control group received a normal diet and free purified water. The modeling phase lasted 8 weeks, during which NAFLD progression was monitored by evaluating parameters such as body weight, blood cholesterol levels, glucose tolerance, insulin resistance, and liver fat accumulation. Adjustments were made as necessary to ensure consistent model establishment. Upon conclusion of the 8-week modeling phase, the NAFLD mice ($n = 40$) were subdivided into four treatment groups ($n = 10$), including HFD group, HFD + CRA-H group (40 mg/kg CRA), HFD +

CRA-L group (20 mg/kg CRA), and HFD + MET group (300 mg/kg MET). Mice in the CRA and MET treatment groups administered daily via intragastric route their respective doses for another 8 weeks. CRA was dispersed in 0.5% sodium carboxymethyl cellulose. Control and Model mice were administered equivalent volumes of 0.5% sodium carboxymethyl cellulose. Throughout the experiment, mice body weight was recorded weekly. After the final treatment, serum, feces, small intestine, fat, and liver samples were collected at –80℃. Liver tissues and small intestines were preserved. All experimental protocols received approval from the Animal Ethics Committee of Guangzhou University of Chinese Medicine (License No: ZYD-2023-231).

2.3. H&E, oil red O staining, and transmission electron microscopy

The white adipose tissue, small intestine, and liver samples were fixed in 4% paraformaldehyde and subjected to paraffin embedding following a gradient dehydration process. Tissue sections, including liver and adipocyte samples, were cut into 5 m slices and stained with hematoxylin and eosin (H&E) for morphological evaluation. For liver oil red O staining, the sections were first rinsed with phosphate-buffered saline (PBS) and counterstained with hematoxylin solution. After 12 min incubation in 60% isopropanol, the sections were treated with oil red O staining solution, based on the manufacturer's protocol. Subsequently, the liver sections were rinsed with water and examined microscopically using an Olympus microscope (TKY, Japan).

Liver samples were collected and immediately fixed in 2.5% glutaraldehyde in 0.1 M PBS (pH = 7.4) at 4℃ for 2 h. Following fixation, tissues were washed in PBS and post-fixed in 1% osmium tetroxide for 1 h. Samples were then dehydrated through a graded ethanol series and embedded in epoxy resin. Ultrathin sections (50 nm) were cut using an ultramicrotome and stained with uranyl acetate and lead citrate. Sections were observed under the HITACHI transmission electron microscope (TKY, Japan), operating at 80 kV. Images were captured for analysis of ultrastructural features.

2.4. Germ-free mice preparation

To deplete gut bacteria in specific pathogen-free (SPF) mice, an antibiotic cocktail comprising ampicillin (1 g/L), neomycin (1 g/L), metronidazole (1 g/L), and vancomycin (0.5 g/L) was prepared in sterile distilled water at the specified concentrations[1]. This cocktail targeted a broad range of Gram-positive and Gram-negative bacteria. Mice were given free access to sterile water with antibiotics for 10 days. Control group mice received an equal volume of sterile distilled water on the same schedule. On day 10, fecal samples were collected, and DNA was extracted to confirm bacterial depletion via agarose gel electrophoresis. All experimental procedures were approved by the Animal Ethics Committee of Guangzhou University of Chinese Medicine (License No: ZYD-2024-261).

2.5. Fecal microbiota transplantation (FMT) to germ-free mice

After antibiotic treatment, Control group mice were maintained on a normal diet, while the Model group received a high-fat diet (HFD) for 8 weeks. Subsequently, mice in both groups were randomized (n = 10 per group) and subjected to daily oral gavage with fecal suspensions derived from either Control or CRA-treated

mice. For FMT preparation, 1 g of feces was suspended in 5 mL sterile PBS and homogenized for 5 min. The suspension was centrifuged at 800 × g for 5 min at 4℃, and the supernatant was collected. Mice were sacrificed at week 16 following FMT for downstream analyses.

2.6. Biochemical index detection

The newly collected mouse blood was left at room temperature for 2 h and centrifuged at 3000 r/min at 4℃ for 10 min. Serum was collected in sterile, enzyme-free tubes. The contents of TG, TC, AST, ALT, LDL-C, and HDL-C in serum were determined according to the instructions of the kits.

2.7. 16S rRNA gene sequencing analysis

Fecal samples were collected on the day before the experiment ended in mouse intestines from three groups and subjected to 16S rRNA gene sequencing. This procedure followed established protocols. Genomic DNA was extracted from 18 fecal samples using HiPure Stool DNA Kits. Then, amplified DNA was purified, quality-checked, and the resulting PCR products were prepared using the NEXTFLEX Rapid DNA-Seq Kit. Sequencing was conducted on the Illumina 2500 platform by Gene Denovo Bio-Tech Co., Ltd. (Guangzhou, China). Purified amplicons were pooled in equimolar concentrations and analyzed via paired-end sequencing, adhering to standard protocols. Data analysis was performed using the OmicShare platform (https://www.omicshare.com). The raw sequencing reads had been deposited in the NCBI Sequence Read Archive accession number: PRJNA843651.

2.8. SCFAs metabolomic analysis

Fecal and liver samples (approximately 0.1 g per sample) were homogenized and weighed, then mixed with 1 mL of PBS and vortexed thoroughly. The mixture was centrifuged at 12,000 r/min for 10 min, and the supernatant was collected. An equal volume of internal standard solution (containing 2-ethylbutyric acid) was added to the supernatant for further analysis. SCFAs were analyzed using a GC, Agilent 7890B equipped with a flame ionization detector (FID) and an ADB-FFAP capillary column (30 m × 0.25 mm, 0.25 m; Agilent Technologies). The injector and detector temperatures were set to 250℃ and 300℃, respectively. The oven temperature was programmed as follows: initial temperature of 60℃ (held for 2 min), ramped to 140℃ at 10℃/min (held for 2.5 min), and further ramped to 200℃ at 10℃/min. Helium served as the carrier gas at a constant flow rate of 1.0 mL/min. SCFAs were identified by comparing their retention times with those of authentic standards. Quantification was based on peak areas relative to the internal standard (2-ethylbutyric acid), and calibration curves were established for acetic acid, propionic acid, butyric acid, isobutyric acid, valeric acid and pentanoic acid.

2.9. Transcriptome sequencing and bioinformatics analysis

Whole-genome transcriptome sequencing was performed by Metware Company (Wuhan, China). Total RNA was extracted from colon tissue using TRIzol reagent. RNA quality and quantity were evaluated using a NanoDrop 2000 spectrophotometer, BioWest agarose gel electrophoresis, and a 5300 Bioanalyzer (SC, USA). Library preparation and RNA sequencing were conducted on the Illumina® strand (CA, USA). Differentially

expressed genes (DEGs) were identified using DESeq2, edgeR, or Limma algorithms with thresholds of Bonferroni-corrected $P \leq 0.05$. Enrichment analysis of DEGs was conducted using Gene Ontology (GO) terms and metabolic pathways, while KEGG pathway analysis was performed with KOBAS-i (Beijing, China).

2.10. Cell experiment

The HepG-2 cell line was obtained from Pricella Biotechnology (Wuhan, China) and cultured in high glucose medium complete medium at 37℃ in a humidified incubator with 5% CO_2. Mycoplasma contamination detection and cell line identification were performed prior to use. HepG2 cells were seeded in 96-well plates and treated with 100 M oleic acid (OA) for 24 h[17]. Cells were subsequently incubated following SCFAs (acetic acid: propionic acid: butyric acid = 1:0.39:0.23) treatment at different concentrations for an additional 24 h. Cell viability was assessed using the CCK-8 assay kit. Oil red O staining was performed according to Solarbio's protocol (Beijing, China).

2.11. Western blot analysis

Liver and cell tissues were homogenized in RIPA buffer containing 1 mmol/L PMSF and centrifuged at 10,000 r/min for 10 min at 4℃ to extract total proteins. The supernatant was subjected to SDS-PAGE for protein separation, followed by transfer onto polyvinylidene difluoride membranes. Membranes were blocked with a blocking solution for 2 h and subsequently incubated overnight at 4℃ with primary antibodies targeting NLRP3, cGAS, STING, p-STING, GSDMD, IL-1β, and GAPDH. After extensive washing with TBST, membranes were incubated with the corresponding secondary antibodies for 2 h at room temperature. Protein bands were visualized using enhanced chemiluminescence reagent and quantified accordingly.

2.12. RT-PCR

To assess mRNA expression levels, total RNA was extracted from frozen mouse liver tissues using Trizol reagent (CA, USA). cDNA synthesis was carried out with the PrimeScript RT kit, and relative quantitative PCR (RT-qPCR) was performed using the SYBR Green PCR kit (CWBIO, Jiangsu, China) following the manufacturer's protocols. The mRNA expression levels were normalized to GAPDH and calculated based on the signal intensity of each target gene. The primer sequences used for real-time PCR were listed in Table 1.

Table 1 Primer Sequences for RT-PCR

Primer	Forward	Reverse
GPR43	GCTGACAGGCTTCGGCTTCTAC	CAGAGCAGCGATCACTCCATACAG
mtDNA	GCGCGGGTTCACGTATACTA	CACGTGGCAACTGTTGTCTG
PINK1	TTGGACAAGATGATCGCCTG	ACACAGATGCCCCTTAGTCT
Parkin	AGGCCTGGATGACTAAACCT	GTGTCAGAATCGACCTCCAC
LC3-II	GAGACATTCGGGACAGCAAT	CTATGTGGGTGCCTACGTTC
NLRP3	CTGGCATCTGGGGAAACCT	TCCTTAGGCTTCGGTCCACA
cGAS	GGGATGGTGAAAGGGGTTGT	TGCTCATAGTAGCTCCCGGT

GSDMD	TAAACTGGGCGGAGGGATGA	CCAGAAGTGTTGAGGGCAGAA
STING	CTGACCCCAACATTCGCTTC	GTCATCTGCAGGTTCCGCTG
IL-1β	AAACCTTTGACCTGGGCTGT	AAGGTCCACGGGAAAGACAC
GAPDH	CGACATACTCAGCACCAGCATCAC	ACGGCAAGTTCAACGGCACAG

2.13. Statistical analysis

The data were presented as mean ± SEM, with all statistical analyses and graphical representations conducted using SPSS 24.0 (NY, USA) and GraphPad Prism ver 6.0 (CA, USA). Group differences were assessed via one-way analysis of variance (ANOVA), followed by Tukey's post hoc test for multiple comparisons. A value of $P \leq 0.05$ was considered statistically significant.

3. Results

3.1. CRA suppressed body weight increase and adiposity in NAFLD mice

Animals were first fed a HFD ad libitum (Fig. 1A for the structural formula) for 8 weeks, and the specific experimental design process was shown in Fig. 1B. CRA significantly inhibited the growth of the body weight, liver weight, and epididymal white adipose tissue weight in NAFLD mice (Fig. 1C-E). HFD certainly leads to weight gain[18, 19], and it also indicates that our animal modeling is successful. The detailed process of the weight recording of the mice was shown in Fig. 1F. The results of the Nuclear Magnetic Resonance Spectroscopy signal confirmed that in comparison to the Controls, the distribution area of white fat on the body surface of the Model group was larger, while the distribution area of white fat on the body surface of NAFLD mice was reduced after different doses of CRA and MET administration (Fig. 1G).

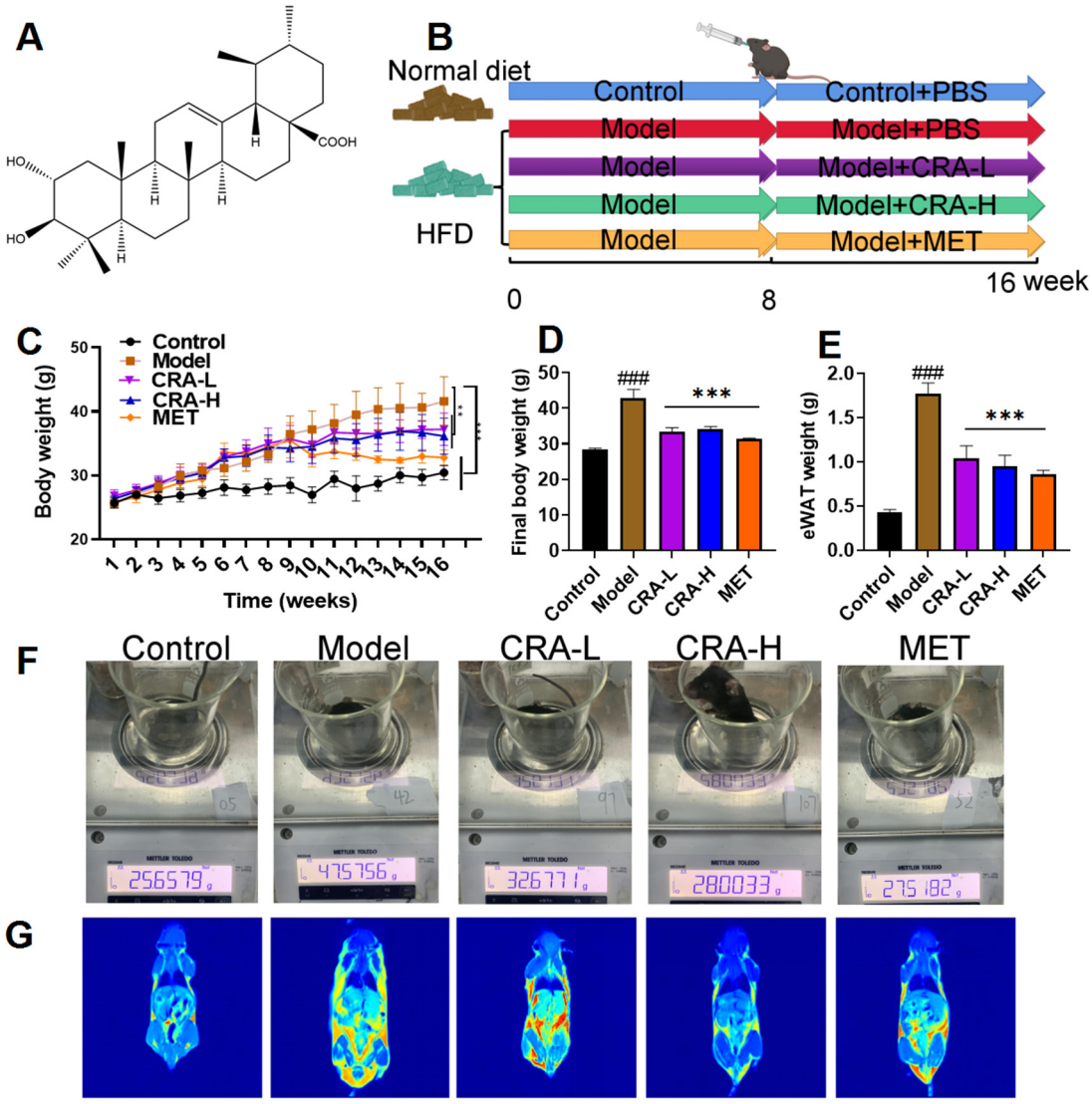


Fig. 1. CRA inhibited weight and fat gain in NAFLD mice. (A) CRA chemical structure formula. (B) Flow chart of animal experiment design. (C) Weight change. (D) Liver weight/weight change. (E) eWAT weight. (F) Weight weighing record. (G) Fat NMR imaging. Data were presented as mean ± SEM (n = 6). $^{\#}P < 0.05$, $^{\#\#}P < 0.01$, $^{\#\#\#}P < 0.001$, compared with Control group; $^{*}P < 0.05$, $^{**}P < 0.01$, $^{***}P < 0.001$, compared with Model group.

3.2. The impact of CRA on lipid profiles and hepatic function in NAFLD mice

Serum concentrations of LDL-C, HDL-C, TG and TC are clinically utilized to evaluate the degree of lesion and the therapeutic efficacy with NAFLD through the changes of these levels[20]. To thoroughly examine the regulatory consequences of CRA on these parameters in a murine model of NAFLD mice, we initially examined gross changes in fatty lesions-related organizations. The findings indicated that the liver and white adipose tissues were markedly enlarged in the NAFLD Model group relative to the Control group and the groups administered varying dosages of CRA or MET (Fig. 2A-B). Analysis of serum lipid indexes revealed that, relative to the Controls, the contents of TG, TC, and LDL-C were upregulated while HDL-C was downregulated in the Models. These dyslipidemic changes were significantly ameliorated to varying degrees following intervention with different doses of CRA or MET (Fig. 2C-F). Interestingly, the lipid-lowering effect of CRA showed a dose-dependent relationship. Meanwhile, the indicators ALT and AST in different dose groups of CRA and MET were significantly reduced in NAFLD mice, suggesting that both

interventions could alleviate NAFLD-induced liver impairment (Fig. 2G-H). Given that NAFLD was associated with impaired glucose metabolism, we subsequently investigated whether CRA could improve glucose tolerance in NAFLD mice. Glucose tolerance experiments confirmed this hypothesis. The results (Fig. 2I) showed that administration of different doses of CRA and MET, significantly improved the sensitivity of NAFLD mice to glucose ($P < 0.001$) compared to the Model group. In summary, different doses of CRA effectively attenuated weight gain and mitigated the elevation of lipid levels, particularly TG and LDL-C, in NAFLD mice.

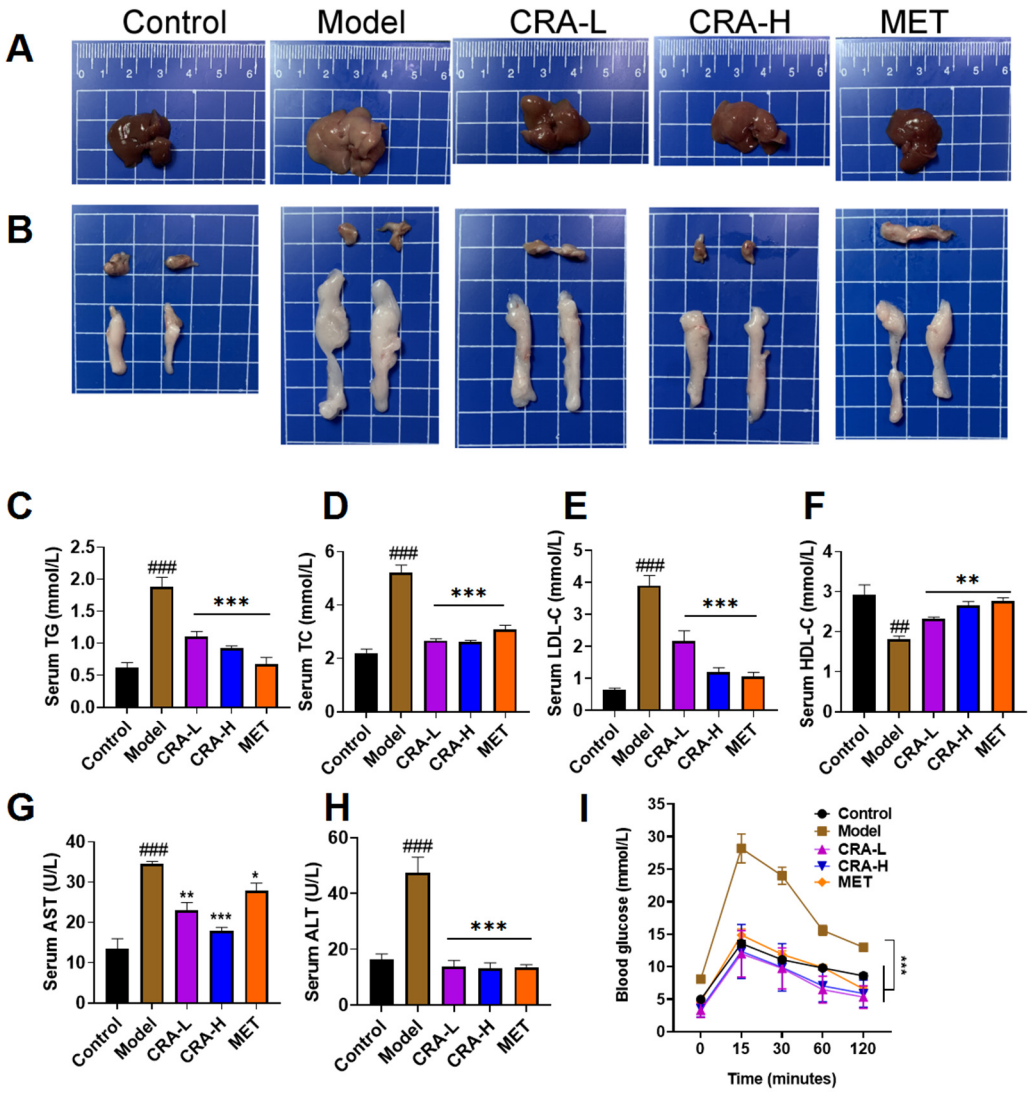


Fig. 2. CRA relieved the symptoms of NAFLD. Sampling recording of the liver (A) and fat (B). Level of serum TG (C), TC (D), LDL-C (E), HDL-C (F), AST (G), and ALT (H). (I) Change of blood glucose. Data were presented as mean ± SEM (n = 6). $^{\#}P < 0.05$, $^{\#\#}P < 0.01$, $^{\#\#\#}P < 0.001$, compared with Control group; $^{*}P < 0.05$, $^{**}P < 0.01$, $^{***}P < 0.001$, compared with Model group.

3.3. CRA reduced liver lipid accumulation and protected intestinal integrity in NAFLD mice

The distribution of liver lipid droplets was one of the important indicators to measure the recovery of NAFLD[19, 21]. In Fig. 3A-B, the lipid accumulation in the liver of Models mice was obvious, which appeared as holes in the tissue surface in the liver HE results and red oil droplet enrichment in the liver oil red O staining. Giving CRA and MET, the liver fat distribution of the mice was significantly reduced (Fig. 3E).

Under high-power microscopy (20-40 ×), HE results of white adipose tissue showed that compared with Control, the adipocytes of white adipose tissue in Model group were squeezed around polygons, with small nuclei and less cytoplasm, which could be reversed after different doses of CRA and MET administration (Fig. 3C). Significantly, we observed that the small intestine of the NAFLD mice suffered severe structural damage, mainly manifested as small intestinal villi breakage or loss, separation of the muscle and serosal layers, and even local necrosis and perforation. In contrast, after giving different doses of CRA and MET, intestinal villi were structurally intact, the muscular layer and serous membrane were closely connected and separated, and the intestinal lamina propria was structurally intact (Fig. 3D, F). The aforementioned results indicated that CRA could reduce the hepatic lipid levels and prevent intestinal injury, which was destroyed by HFD.

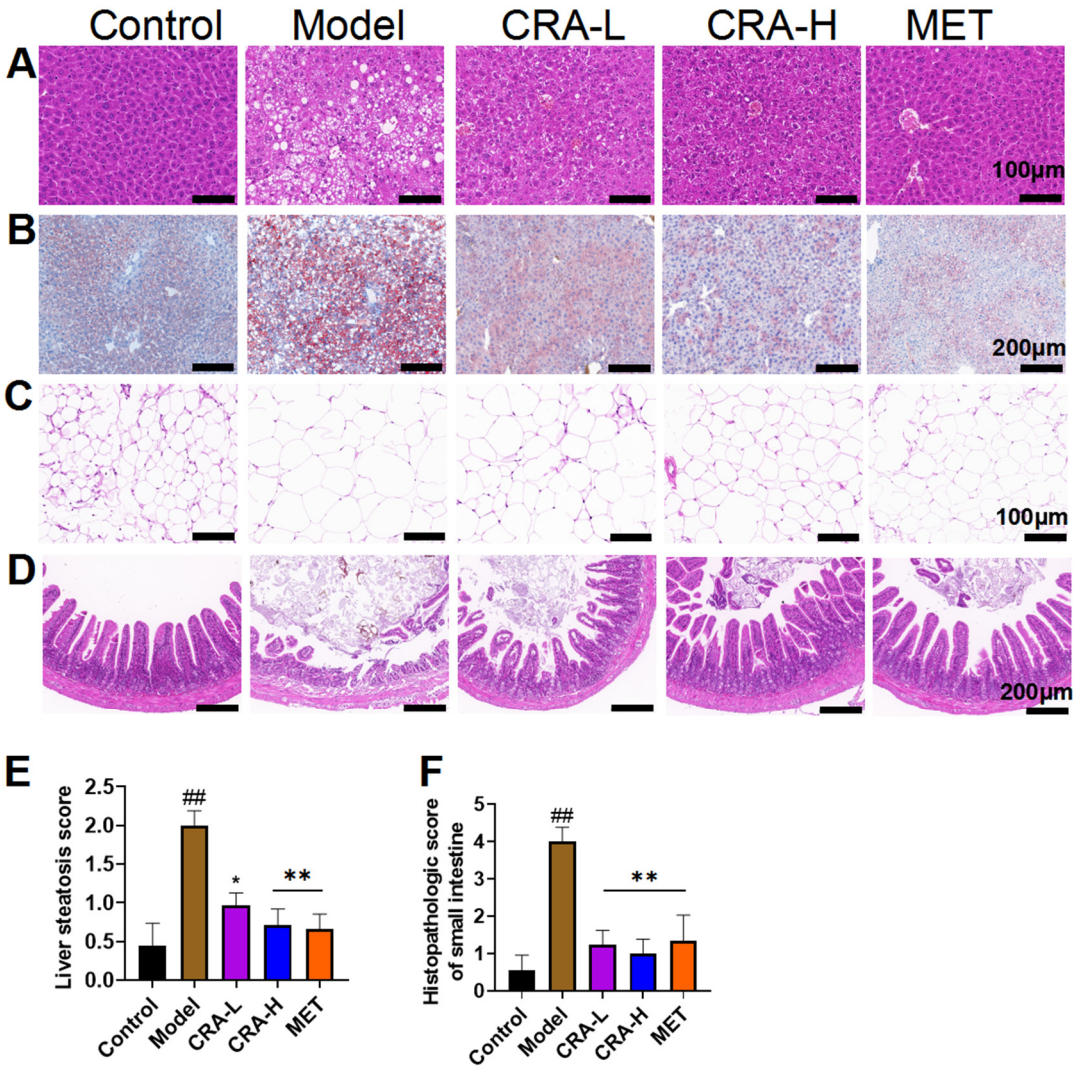


Fig. 3. Representative histological results of H&E and Oil Red O staining. (A) Liver H&E staining. (B) Liver Oil Red O staining. (C) White fat H&E staining. (D) Small intestine H&E staining. (E) Liver steatosis score. (F) Histopathologic score of small intestine. Data were presented as mean ± SEM ($n = 3$). $^{\#}P < 0.05$, $^{\#\#}P < 0.01$, $^{\#\#\#}P < 0.001$, compared with Control group; $^{*}P < 0.05$, $^{**}P < 0.01$, $^{***}P < 0.001$, compared with Model group.

3.4. CRA regulated gut microbiota structure in NAFLD mice

Intestinal microenvironment homeostasis dysbiosis may promote the development of NAFLD by increasing the abundance of harmful bacteria producing substances that damage to the intestinal. As shown in

Fig. 4A, the result of PCoA indicated that the composition and structure of the three groups of bacteria were different. Specifically, CRA upregulated the Shannon and Chao1 indexes in the gut of NAFLD mice, suggesting that CRA alleviated NAFLD by regulating gut microbiota (Fig. 4B-C). Next, we continued to focus on the specific changes in which bacteria in the gut of NAFLD mice were regulated by CRA. At the phylum level, the relative abundance of Firmicutes in the NAFLD mice was up and Bacteroidota was down. As expected, CRA reduced the Firmicutes/Bacteroides ratio to a normal level (Fig. 4D). Similarly, at the genus level, compared with the Controls, relative proportion of *Candidatus_Saccharimonas*, *Lachnoclostridium*, *Ileibacterium*, and *Colidextribacter* was upregulated in the Model group, but reversed after CRA administration. In addition, the relative abundance of *Prevotellaceae_UCG-001*, *Lactobacillus*, *Bacteroides*, and *Lachnospiraceae_NK4A136_group* were decreased in the gut of NAFLD mice, while reversed by CRA (Fig. 4E). This also explained the previous effect of CRA on improving the intestinal mucosal barrier.

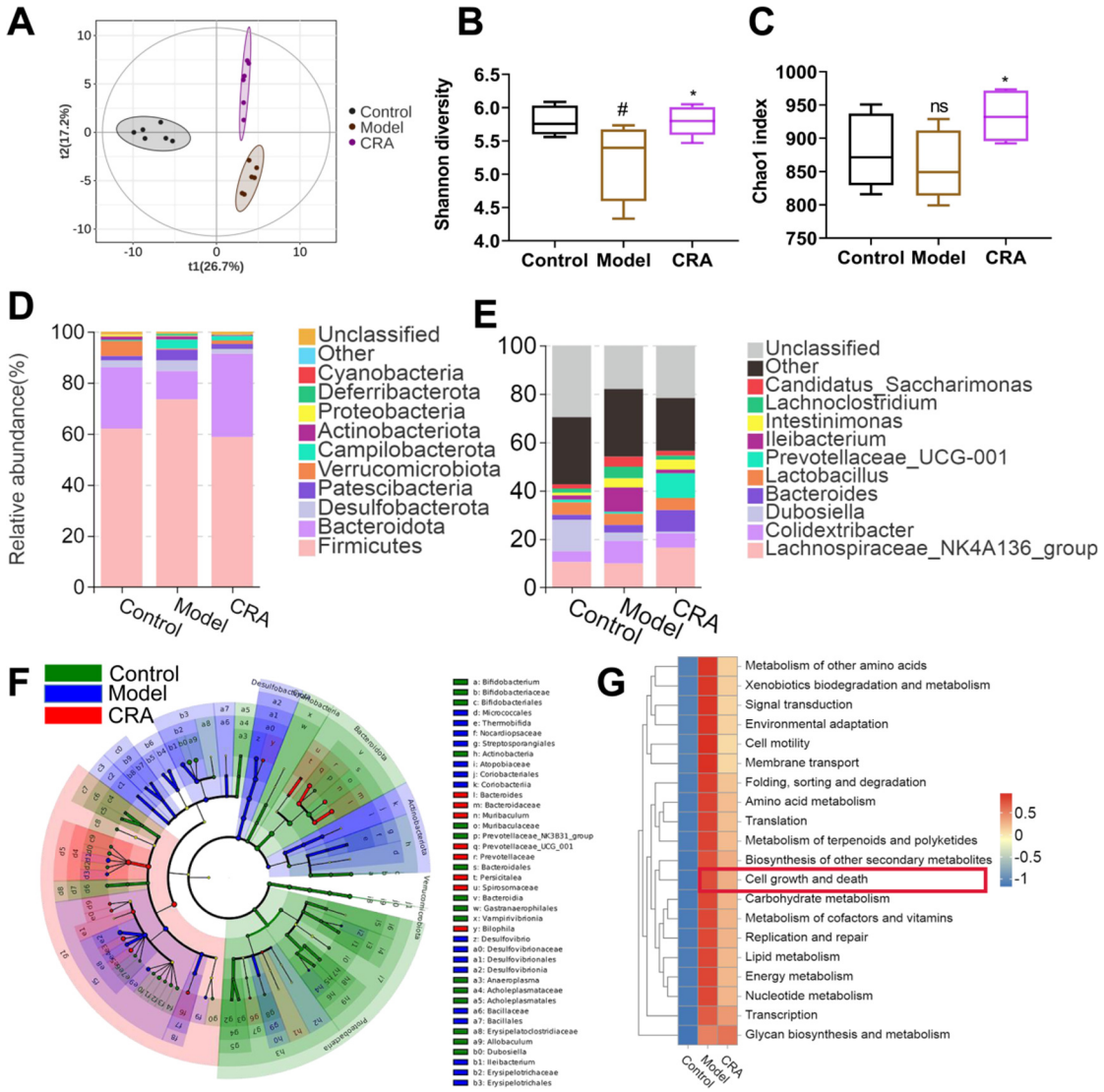


Fig. 4. CRA regulated the gut microbiota of NAFLD mice. (A) PCoA analysis. (B) Shannon index. (C) Chao1 index. Bacterial species abundance at phylum (D) and genus level (E). (F) LDA value distribution histogram at genus level. (G) Functional abundance heat map (level 2). Data were presented as mean ± SEM (n = 6). $^{\#}P < 0.05$, compared with Control group; $^{*}P < 0.05$, compared with Model group.

More specifically, bacterial taxa uniquely enriched across different interventions were meticulously characterized by linear discriminant analysis effect size (LEfSe), yielding a comprehensive clade map alongside an LDA score distribution. Collectively, 44 specific bacterial taxa with LDA values exceeding 2 were detected, spanning from the phylum down to the genus level (Fig. 4F). Of these, 12 taxa were predominantly enriched in the Controls, 12 in the Models, and 20 in the CRAs. For instance, the Controls displayed an elevated presence of genera such as *Bacteroides* and *Akkermansia*. In contrast, the Model group was distinguished by an increased relative abundance of *Desulfovibrionaceae*, *Ileibacterium*, and *Erysipelotrichaceae*. Meanwhile, the CRA supplementation was distinctly associated with an increased prevalence of the genera *Bacteroides*, *Clostridia*, and *Lachnospiraceae*. Functional abundance heat map results proposed that CRA may be engaged in lipid metabolism, cell growth and death, cell motility, etc. (Fig. 4G). Overall, the treatment of NAFLD by CRA might be related to its involvement in the downregulation of potentially damaging intestinal barrier bacteria, while some potential probiotics producing SCFAs were upregulated, suggesting that gut microbiota were important in the treatment of NAFLD by CRA.

3.5. Fecal microbiota from CRA transplants revealed that the effects of CRA on NAFLD mice were microbiota-dependent

To confirm that the effects of CRA on NAFLD mice were microbiota dependent, fecal samples were collected from mice in CRA-H, and the design of the FMT experiment was illustrated in Fig. 5A. As demonstrated in Fig. 5B, FMT effectively prevented weight augmentation in NAFLD mice. In the Models, the liver showed a pale, oily, and hypertrophic appearance (Fig. 5C1), and histological analysis revealed multiple vacuolar lesions in H&E-stained sections (Fig. 5C2), while the intestinal villi showed damage and the mucosal barrier structure was disrupted (Fig. 5C3). Interestingly, post-FMT treatment reversed these conditions, restoring liver morphology and intestinal integrity to levels similar to the Control group.

Additionally, eWAT weight was substantially raised ($P < 0.001$) in NAFLD mice in comparison to the Control, but this increase was notably inhibited by FMT (Fig. 5D). In terms of, markers such as TG, TC, and LDL-C were elevated in the Models while significantly reduced in both the Control and FMT groups (Fig. 5E-G). Meanwhile, FMT could also improve NAFLD-induced insulin resistance markedly (Fig. 5I-J). Collectively, these results underscored that the ramifications of the CRA on NAFLD were largely mediated by microbiota alterations, indicating the potential of microbiome-targeted therapies for the treatment of NAFLD.

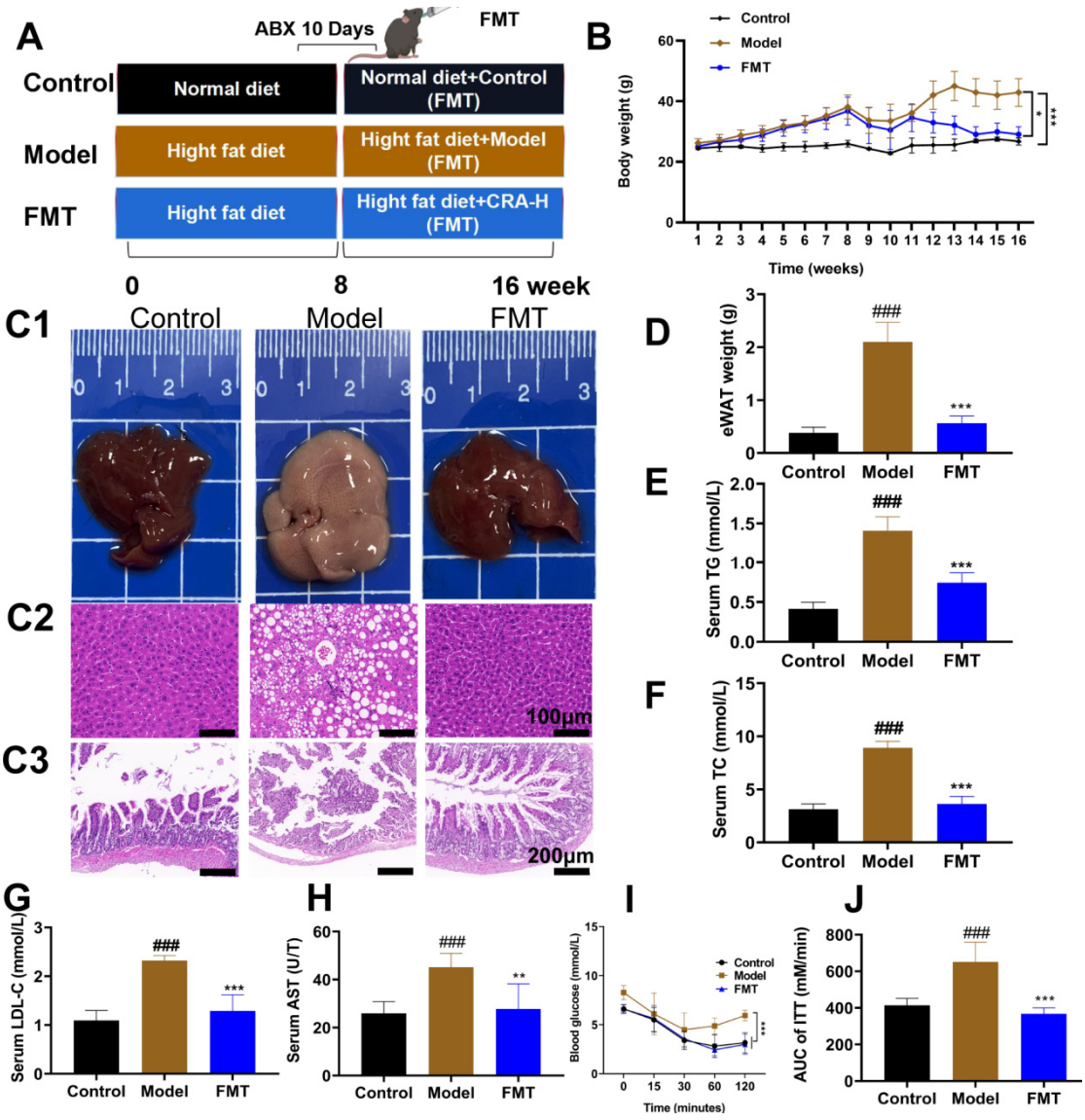


Fig. 5. Efficacy verification of FMT. (A) FMT experiment design. (B) Body weight change. (C1) Liver photograph, (C2) H&E staining of the liver, (C3) H&E staining of the small intestine. (D) eWAT weight. (E) Serum TG level. (F) Serum TC level. (G) Serum LDL-C level. (H) Serum AST level. Blood glucose (I) and AUC (J) of ITT. Data were presented as mean ± SEM ($n = 6$). $^{\#}P < 0.05$, $^{\#\#}P < 0.01$, $^{\#\#\#}P < 0.001$, compared with Control group; $^{*}P < 0.05$, $^{**}P < 0.01$, $^{***}P < 0.001$, compared with Model group.

3.6. Effects of CRA intervention on SCFAs profiles in the NAFLD mice

The involvement of gut microbiota in the management of NAFLD by CRA has been substantiated. Numerous studies have indicated that gut bacteria influence the body via promoting the synthesis of SCFAs. To further ascertain whether CRA exerts its therapeutic effects through the regulation of microbiota-derived metabolites, we measured the amounts of SCFAs in mouse feces utilizing gas chromatography. The concentrations of SCFAs in feces and livers were shown in Fig. 6. As expected, the primary SCFAs in all groups included acetate, propionate, butyric acid, isobutyric acid, valeric acid, and isovaleric acid. In fecal samples, the proportions of acetate, propionate, and isobutyric acid were significantly down-regulated in the Models, whereas butyric acid was increased in both the Control and CRA (Fig. 6A, B and D). Although the disparity in isobutyric acid levels comparing the Model and CRA groups was not statistically significant (Fig.

6C), valeric and pentanoic acid levels were markedly elevated in the Model group compared to the Control and CRA (Fig. 6E-F).

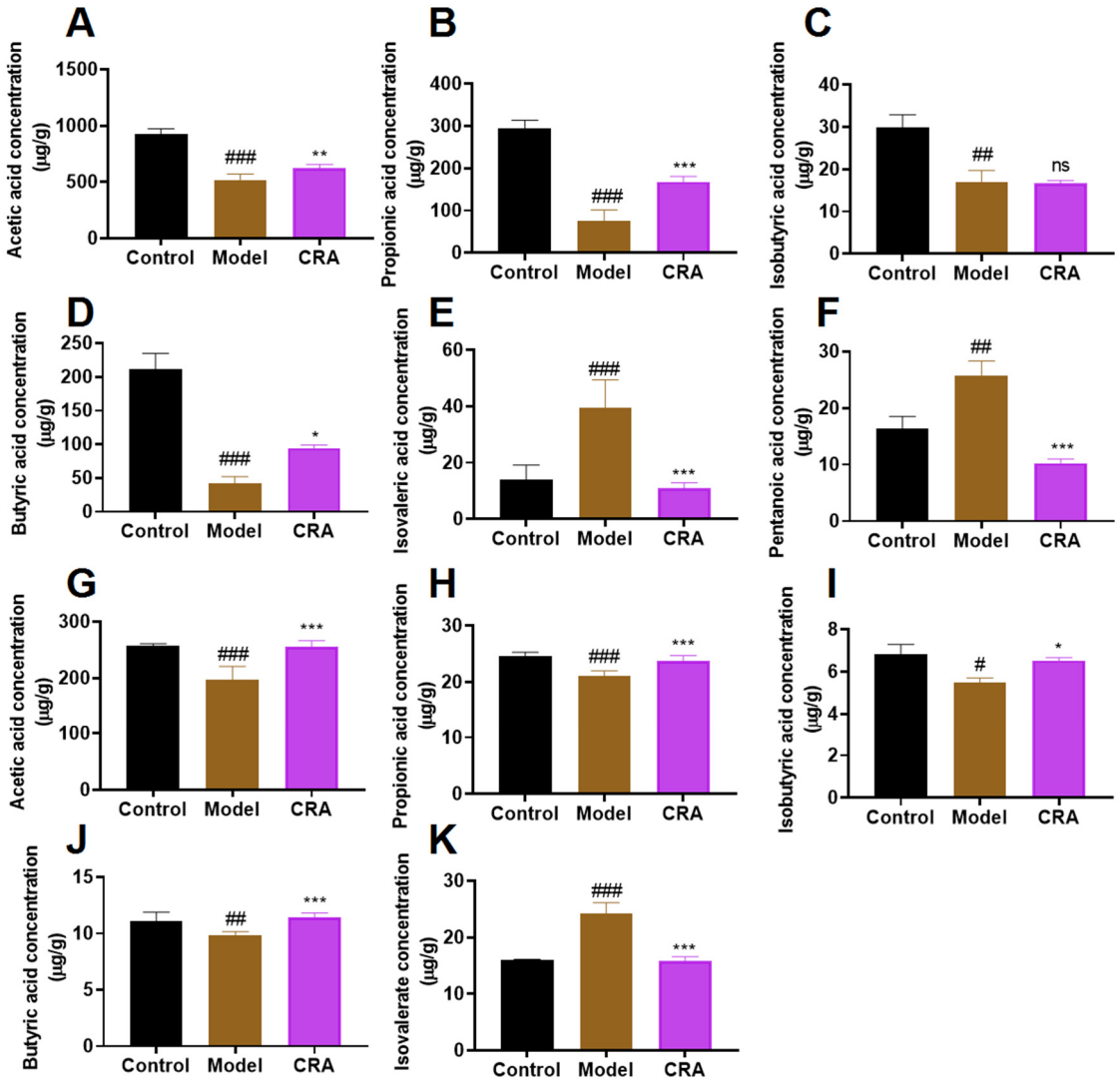


Fig. 6. Effect of CRA on the changes of SCFAs content in feces and livers of NAFLD mice. Fecal concentration of acetic acid (A), propionic acid (B), isobutyric acid (C), butyric acid (D), isovaleric acid (E), pentanoic acid (F). Liver concentration of acetic acid (G), propionic acid (H), isobutyric acid (I), butyric acid (J), isovaleric acid (K). Data were presented as mean ± SEM ($n = 6$). $^{\#}P < 0.05$, $^{\#\#}P < 0.01$, $^{\#\#\#}P < 0.001$, compared with Control group; $^{*}P < 0.05$, $^{**}P < 0.01$, $^{***}P < 0.001$, compared with Model group.

To further verify whether the metabolic profile of SCFAs in the liver was consistent with that in the gut, we subsequently analyzed SCFAs in the mice liver. Specifically, isobutyric acid was significantly increased in the liver of CRA-treated NAFLD mice compared to the Model group, indicating that CRA may promote the potential anti-inflammatory properties of isobutyric acid in the liver via the gut-liver axis. However, valeric acid was undetectable in liver tissue, probably due to its low bioavailability in hepatic tissue, as documented in prior analyses of SCFAs distribution across different organs[22]. Overall, SCFAs contents in feces and liver were analyzed, demonstrating the significant influence of CRA on SCFAs composition and elucidating the possible action of CRA to improve intestinal barrier. Furthermore, the trend of SCFAs in liver was similar to that in feces, suggesting that CRA may modulate the gut-liver axis by altering SCFAs profiles, potentially improving NAFLD symptoms.

3.7. Transcriptomics revealed possible mechanisms of CRA anti-NAFLD

A transcriptome study of the liver was conducted to elucidate the processes by which CRA mitigates NAFLD. Fig. 7A showed that the gene expression patterns of the liver in NAFLD mice changed significantly after CRA treatment, and the gene expression profile in CRA tended to converge with the Controls. To explore the biological functions of these DEGs, we conducted KEGG and GO analyses by querying each group's DEGs in the database. We then acquired the top 20 enriched phrases for both KEGG and GO pertaining to the DEGs. The result of the KEGG analysis was shown in Fig. 7B1-B2. In cellular processes, the three groups were enriched into phagosomes, in which Control versus Model accounted for 4.83% and CRA versus Model accounted for 5.41%. In environmental information processes, cytokine-cytokine receptor interaction was enriched among three groups, among which Control vs. Model accounted for 6.9% and CRA vs. Model accounted for 6.76%. It was evident that phagosome activation and cytokine-cytokine receptor interaction in KEGG revealed the greatest significant disparity among the three groups. These findings suggested that the anti-NAFLD effects of CRA may be involved in cytokine and cytophagocytosis processes.

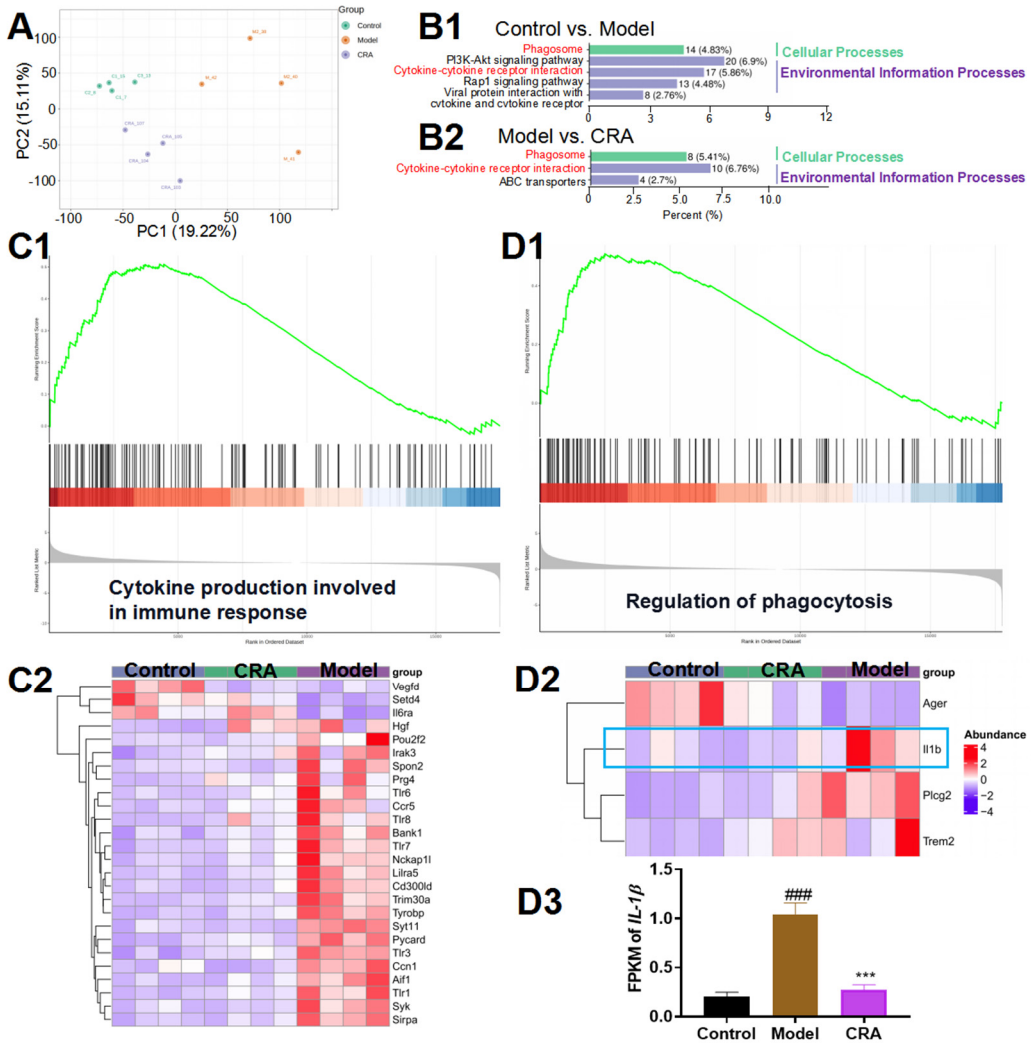


Fig. 7. Transcriptome characteristics of the liver. (A) PCA plot. KEGG enrichment analysis Control vs. Model (B1) and Control vs. Model (B2). GSEA enrichment plots of cytokine production involved in immune response (C1), regulation of phagocytosis (D1). Heat map clustering analysis of cytokine production involved in immune response (C2), regulation of phagocytosis (D2). (D3) FPKM of *IL-1β*. Data were presented as mean ± SEM ($n = 4$). $^{\#}P < 0.05$, $^{\#\#}P < 0.01$, $^{\#\#\#}P < 0.001$, compared with Control group; $^{*}P < 0.05$, $^{**}P < 0.01$, $^{***}P < 0.001$, compared with Model group.

Based on the KEGG and GO enrichment analyses, GSEA was performed on the KEGG and GO datasets to further examine the biological significance of these pathways. As illustrated in Fig. 7C1-D1, cytokine production involved in immunity and phagocytosis was enriched in both the Control vs. Model and CRA vs. Model groups. In detail, there were 26 genes involved in cytokine production in the immune response, of which 22 were downregulated and 4 increased in the CRAs and Controls compared to the Models. The upregulated genes included *Prg4*, *Pou2f2*, *Irak3*, *Syk*, *Nckap1l*, *Aif1*, *Il6ra*, *Ccn1*, *Tyrobp*, *Pycard*, *Trim30a*, *Tlr3*, *Cd300ld*, *Spon2*, *Sirpa*, *Bank1*, *Tlr8*, *Tlr7*, *Tlr1*, *Syt11*, *Lilra5*, and *Ccr5*. Downregulated genes included *Tlr6*, *Setd4*, *Hgf*, and *Vegfd*. In addition, 4 genes involved in the regulation of phagocytosis were *Ager*, *Trem2*, *IL-1β*, and *Plcg2*. Among them, *IL-1β* showed a high expression in the Models (Fig. 7D3). Overall, CRA treatment could significantly improve the liver gene expression profile of NAFLD mice, which resembled of Controls. Through KEGG and GO enrichment analysis, it was found that the anti-NAFLD effect of CRA was closely related to immune regulatory processes related to cytokines and phagocytosis.

3.8. CRA regulated cGAS-STING signaling pathway in NAFLD mice

When mitophagy was impaired, mtDNA exposed to the cytosol could be recognized by cyclic GMP-AMP synthase (cGAS), leading to the activation of the cGAS-STING signaling pathway. This activation triggered the production of type I interferons and pro-inflammatory cytokines, promoting inflammation and the development of related diseases such as autoimmune disorders and chronic inflammatory conditions[10]. Therefore, we investigated the SCFAs regulated by CRA on mitochondria. According to electron microscopy (EM) images, liver tissue from NAFLD mice showed disturbed mitochondrial structures characterised by mitochondrial swelling. In contrast, CRA treatment not only preserved mitochondrial integrity but also increased mitochondrial number (Fig. 8A). To further assess mitochondrial damage, we measured mtDNA levels in the mice liver. Elevated mtDNA in liver by RT-PCR indicated extensive hepatocyte necrosis or apoptosis accompanied by mitochondrial damage, whereas CRA treatment markedly mitigated this injury, effectively protecting against HFD-induced mitochondrial damage (Fig. 8B). *GPR43* mediated the beneficial effects of SCFAs and Ca^{2+} on metabolic health, potentially mitigating NAFLD by regulating calcium signaling pathways, gut-liver axis modulation, and improving energy homeostasis[23]. Compared to the Control group, the Model group had significantly down-regulated *GPR43* gene expression, yet CRA intervention reversed this change (Fig. 8C). Ca^{2+} played a critical role in mitochondrial function and dynamics. Specifically, elevated mitochondrial Ca^{2+} levels could stimulate mitochondrial biogenesis, including mtDNA replication[24]. In Fig. 8D, Ca^{2+} was found to be elevated in NAFLD mice's liver but significantly down regulated in the CRA. The results of RT-PCR also showed that CRA could significantly reduce the levels of *PINK1*, *Parkin* and *LC3-II* in the liver of NAFLD mice (Fig. 8E-G). These results suggested that intracellular Ca^{2+} and mtDNA levels were regulated by CRA.

To further explore whether the treatment of NAFLD by CRA could regulate the hepatic cGAS-STING, we used Western blot to detect key proteins. The findings indicated the comparative expression of the hepatic proteins NLRP3, cGAS, GSDMD-FL, GSDMD-N, p-STING, pro-IL1β, and mature-IL1β had significant

upregulation in the Model group. However, the CRA could significantly lower expression of these proteins (Fig. 8H-O). In conclusion, CRA alleviated NAFLD by suppressing the cGAS-STING pathway to reduce liver inflammation, demonstrating protective effects against liver injury.

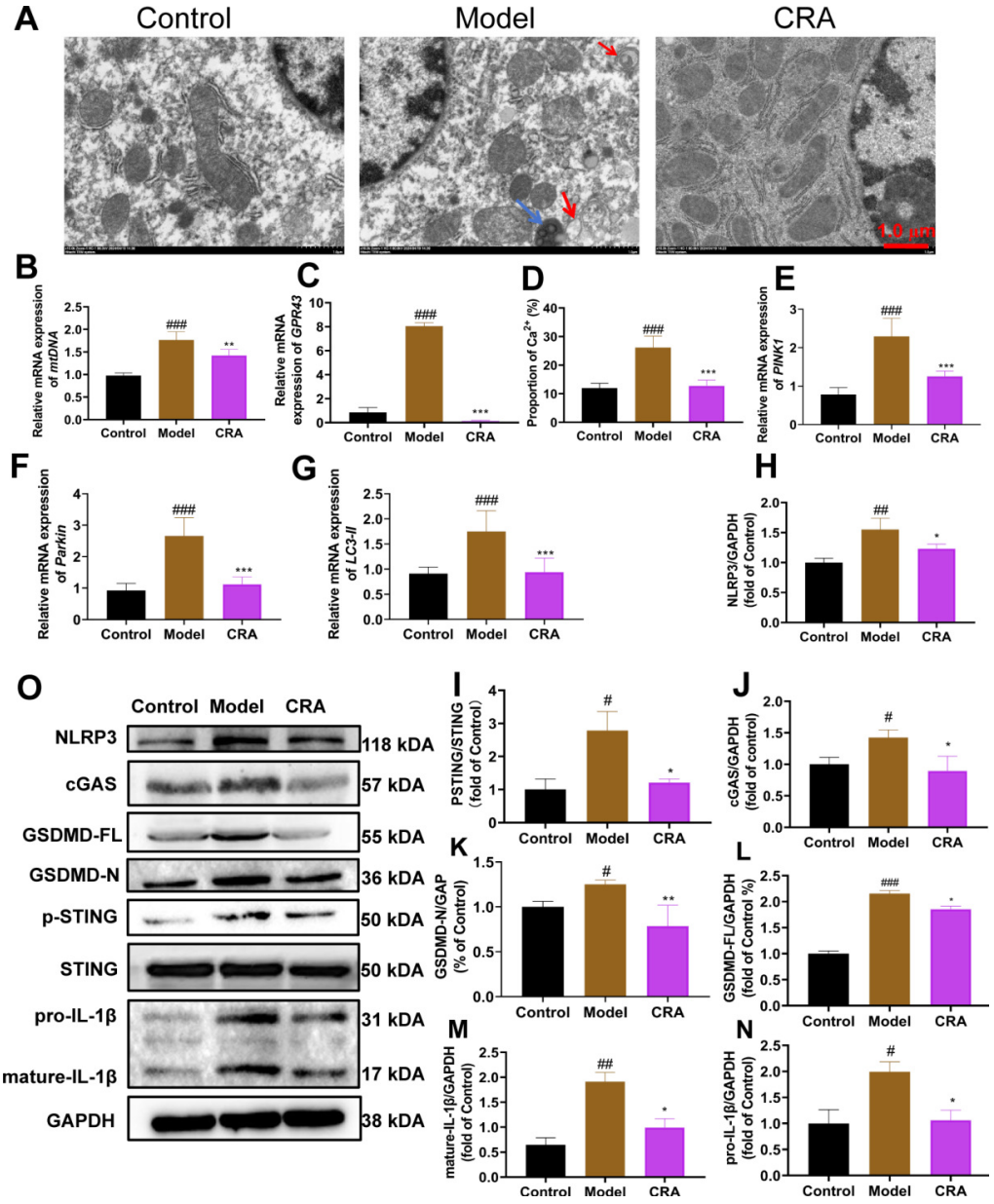


Fig. 8. Liver mitochondrial electron microscope and Western blot. (A) Liver mitochondrial electron microscope (the blue arrow: the autophagosome; the red arrow: mitochondrial autophagy). Relative mRNA expression of *mtDNA* (B), *GPR43* (C), *PINK1*, *Parkin*, and *LC3-II*. Proportion of Ca^{2+} (D). Relative protein expression of NLRP3 (H), cGAS (I), GSDMD-FL (J), GSDMD-N (K), p-STING/STING (L), pro-IL-1β (M), mature-IL-1β (N). (O) Representative Western blot analysis for expressions of NLRP3, cGAS, GSDMD-FL, GSDMD-N, p-STING, STING, pro-IL-1β, mature-IL-1β, and GAPDH. Data were presented as mean ± SEM (n = 3-6). $^{\#}P < 0.05$, $^{\#\#}P < 0.01$, $^{\#\#\#}P < 0.001$, compared with Control group; $^{*}P < 0.05$, $^{**}P < 0.01$, $^{***}P < 0.001$, compared with Model group.

3.9. The regulatory effects of SCFAs treatment on NAFLD and inhibition of cGAS-STING signaling pathway in HepG2

SCFAs have been documented to exert therapeutic effects in NAFLD. To investigate whether CRA indirectly influenced the regulation of SCFAs produced by gut microbiota, we examined its efficacy and underlying mechanisms at the cellular level (Fig. 9A). The results showed that cell viability was enhanced by

different doses of SCFAs, among which, 25 M SCFAs was identified as the optimal concentration (Fig. 9B). Consequently, concentrations (12.5, 25 and 50 μmol/L) were selected for subsequent PCR analysis. In the study, levels of TG and TC were high in NAFLD models using HepG2 but were considerably reduced subsequent to SCFAs subsequent to in a dose-dependent manner (Fig. 9C-D). Additionally,, RT-PCR analysis showed that *NLRP3*, *cGAS*, *GSDMD*, *IL-1β* levels rose in the Model group compared to the Control group, while SCFAs treatment markedly reduced these inflammatory markers (Fig. 9E-H). Collectively, CRA may indirectly alleviate NAFLD by regulating gut microbiota to elevate SCFAs production, which in turn suppresses liver inflammation via the cGAS-STING signaling pathway.

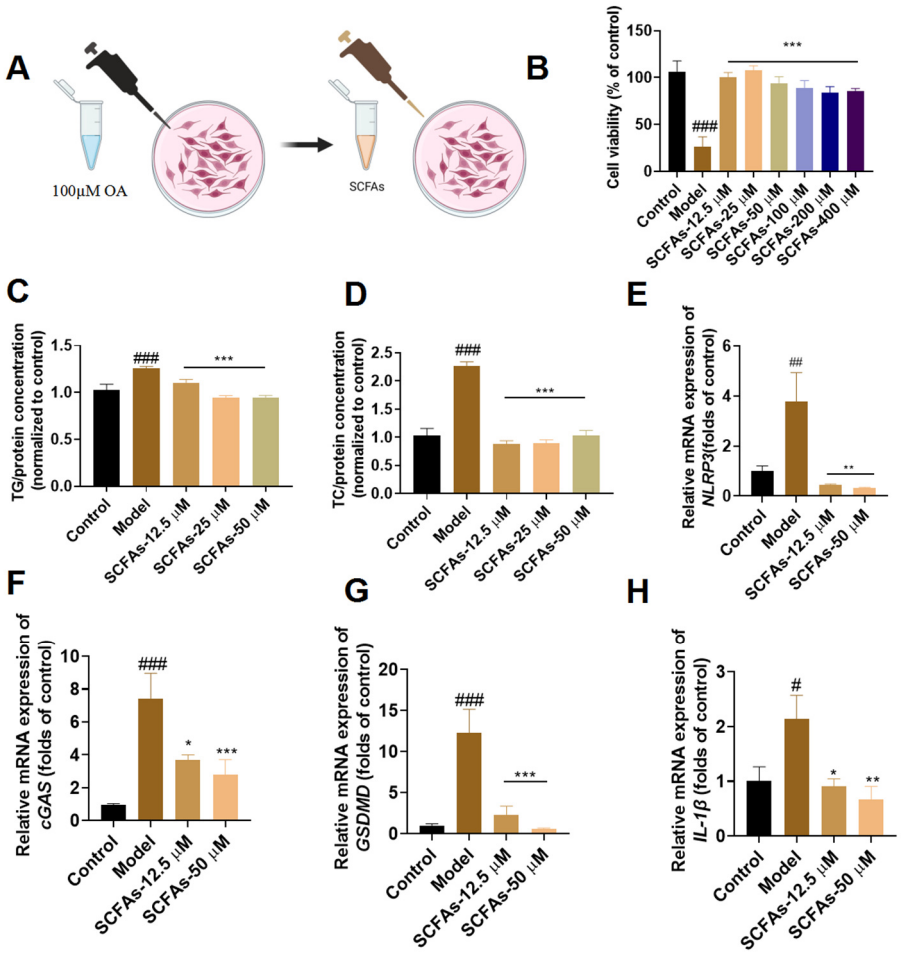


Fig. 9. SCFAs alleviated NAFLD HepG2 through regulated cGAS-STING pathway. (A) Cell experimental design process. (B) Cell viability. Concentrations of TG (C) and TC (D). Relative mRNA expression of *NLRP3* (E), *cGAS* (F), *GSDMD* (G), and *IL-1β* (H). Data were presented as mean ± SEM ($n = 6$). $^{\#}P < 0.05$, $^{\#\#}P < 0.01$, $^{\#\#\#}P < 0.001$, compared with Control group; $^{*}P < 0.05$, $^{**}P < 0.01$, $^{***}P < 0.001$, compared with Model group.

3.10. SCFAs inhibited cGAS-STING pathway key proteins in NAFLD cells via STING protein

To verify whether the impact of SCFAs against NAFLD depended on the cGAS-STING pathway, Western blot and immunofluorescence methodologies were used for detection key proteins in the cGAS-STING pathway. The Western blot findings indicated that the administration of SCFAs substantially decreased the protein expression levels of NLRP3, cGAS, STING, GSDMD, and IL-1β in NAFLD cells (Fig. 10A-E). The typical Western blot bands of each target protein were shown in Figure 10F. Notably, after stimulation with the STING protein agonist DMXAA, the inhibitory effect of SCFAs on the expression of

these proteins was suppressed, and this suppression was dose-dependent (Fig. 10A-E). In addition, the overall trend of the immunofluorescence results was consistent with the Western blot results. The typical immunofluorescence plot is shown in Figure 10F. It indicated that SCFAs could reduce the level of protein manifestation of cGAS, STING, GSDMD, and IL-1β in NAFLD cells, and this effect was mediated through the STING protein (Fig. 10 G-J). Collectively, the findings presented in the text were highly significant in understanding the protective role of SCFAs in NAFLD. The use of Western blot and immunofluorescence techniques to detect principal makers in the cGAS-STING pathway provides reliable evidence for the research. In summary, SCFAs may bind to certain receptors or components related to the STING protein to exert their inhibitory effect.

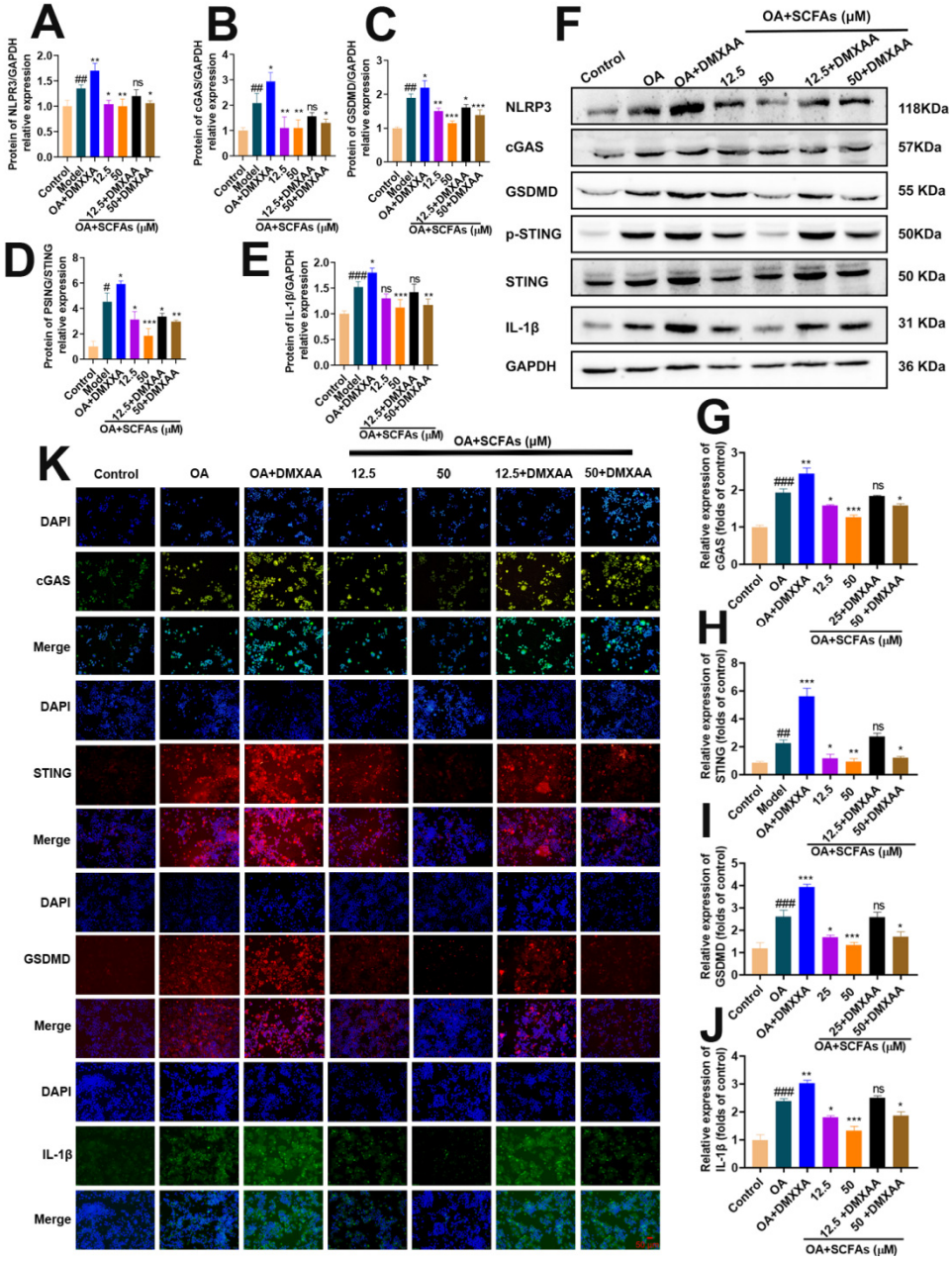


Fig. 10. SCFAs modulated the cGAS-STING signaling axis to mitigate cellular pathophysiology in NAFLD. Relative expressions of NLRP3 (A), cGAS (B), GSDMD (C), STING (D), IL-1β (E). Typical Western blot bands (F). Cellular immunofluorescence characteristic figures (K). Positive expression areas of cGAS (G), STING (H), GSDMD (I), and IL-1β (J) in immunohistochemistry. Data were presented as mean ± SEM (n = 3-5). $^{\#}P < 0.05$, $^{\#\#}P < 0.01$, $^{\#\#\#}P < 0.001$, compared with Control group; $^{*}P < 0.05$, $^{**}P < 0.01$, $^{***}P < 0.001$, compared with Model group.

4. Discussion

The rising prevalence of HFD, characterized by frequent consumption of fried foods, fatty meats, and fast food, has become a significant public health concern due to changing lifestyles and the rapid expansion of the fast-food industry. NAFLD is one of the most common health problems associated with HFD. NAFLD is closely linked to gut dysbiosis, this may result in heightened intestinal permeability and inflammation, thereby promoting the progression of the disease[3]. In recent years, various natural compounds have shown potential in alleviating NAFLD. CRA, a natural compound found in fruits such as eriobotrya japonica, hawthorns, and actinidia[13, 25, 26], has received much acknowledgment for its promising applications in improving obesity, immune disorders, and liver cancer[13, 27]. Although previous research has highlighted the health benefits of these fruits, few studies have specifically examined the effects of CRA in the treatment of HFD-induced NAFLD, with the underlying processes remaining ambiguous. Traditional Chinese medicines (TCMs) with the property of "food and medicine homology" mostly participate in the prevention of NAFLD through a "multi-component, multi-target, and multi-pathway" mode[28]. Therefore, this research seeks to investigate the therapeutic benefits of CRA on HFD-induced NAFLD and elucidate its potential mechanism of action, which is of immense significance for both food science and human health.

Our findings demonstrated that CRA inhibited HFD-induced body weight gain, and reduced the concentrations of TG, TC, HDL-C, LDL-C, AST, and ALT, while enhancing glucose tolerance and insulin sensitivity in NAFLD mice. These findings were consistent with prior research[11, 13], positively associated with improvements in NAFLD, and laying the foundation for further exploration of CRA's mechanism of action. Studies have shown that the gut microbiome influences liver health and immune balance primarily through altering the microbiota's makeup, governing gut microbial metabolites, and improving the intestinal barrier function[3, 29]. In our investigation, CRA demonstrated multifaceted therapeutic potential in mitigating NAFLD through its effects on liver lipid accumulation, intestinal integrity, and gut microbiota structure. Specifically, CRA significantly reduced liver lipid accumulation, as evidenced by the decreased distribution of lipid droplets in the liver tissue of NAFLD mice, which is consistent with previous reports that CRA has reduced lipid droplet accumulation in the liver[13]. This reduction in liver fat is crucial for managing NAFLD, as excessive lipid accumulation is a hallmark of the disease and contributes to liver dysfunction. Furthermore, CRA demonstrated protective effects on the intestinal structure of NAFLD mice, preserving the integrity of intestinal villi and the muscular layer, which are often compromised in HFD-induced NAFLD models[30]. The capacity of CRA to safeguard the intestinal barrier is notably important, since heightened intestinal permeability correlates with the advancement of NAFLD and can lead to systemic inflammation.

In addition to its direct effects on liver and intestinal health, CRA was found to modulate the composition of the gut microbiota in NAFLD mice, which is a critical factor in the pathogenesis of the disease. Microbiota dysbiosis in the intestines, marked by an imbalance in bacterial composition, has been associated with the advancement of NAFLD via the facilitation of intestinal barrier failure and inflammation[31]. The findings demonstrated that CRA enhanced gut bacterial diversity and abundance, as indicated by the upregulation of

the Shannon and Chao1 indexes, key indicators used to indicate the changes of intestinal flora in NAFLD[32]. This suggests that CRA can modulate the gut microbiota to a healthier state, this might be a factor in its ability to treat NAFLD. Specifically, CRA reduced the Firmicutes/Bacteroidota ratio, which is often elevated in NAFLD, and reversed the relative abundance of several harmful and beneficial bacterial taxa[33]. The reduction in potentially harmful bacteria, such as *Candidatus_Saccharimonas* and *Ileibacterium*, and the upregulation of beneficial SCFA-producing bacteria, such as *Prevotellaceae_UCG-001*, *Lactobacillus*, *Bacteroides*, and *Lachnospiraceae_NK4A136_group*, highlight the role of CRA in promoting a more favorable gut microbiota profile. SCFAs, particularly acetate, propionic, and butyric acid, are known to maintain gut barrier integrity and exert anti-inflammatory effects, which are essential to the management of NAFLD[34, 35]. *Candidatus_Saccharimonas* is a member of the Candidate Phyla Radiation and is known for its parasitic nature and reduced genome size[36]. It has been associated with various inflammatory conditions and can inhibit TNF production within macrophages, which is linked to inflammatory, lipid metabolism and oxidative diseases[37]. The reduction of *Candidatus_Saccharimonas* in the gut microbiota suggests that CRA may mitigate inflammation and enhance overall gut health. *Ileibacterium* is another potentially harmful bacterium that has been implicated in gut dysbiosis and is associated with intestinal inflammation[38]. The decrease in *Ileibacterium* levels following CRA treatment indicates a potential reduction in gut inflammation and an improvement in gut barrier function. On the other hand, the upregulation of beneficial SCFA-producing bacteria such as *Bacteroides*, *Lachnospiraceae_NK4A136_group, Prevotellaceae_UCG-001*, and *Lactobacillus*, is particularly noteworthy. *Prevotellaceae_UCG-001* and *Lachnospiraceae_NK4A136_group* are potent producers of SCFAs and have shown their host's ability for metabolic wellness[25]. *Bacteroidota* and *Prevotellaceae_UCG-001* were the known dominant bacteria producing acetic acid and butyrate acid [39], *Lachnospiraceae_NK4A136_group* and *Lactobacillus* produce acetate acid, propionate acid, and butyrate acid [40]. The increase in these beneficial bacteria suggests that CRA can modulate the gut microbiota to enhance SCFA production, which in turn can improve gut health and reduce inflammation. Moreover, the results of the FMT experiment further support the notion that the therapeutic effects of CRA on NAFLD are largely mediated by microbiota alterations. The successful use of FMT to prevent weight gain, restore liver morphology, and improve intestinal integrity in NAFLD mice underscores the essential function of gut microbiota in modulating host metabolism and advancement of illness, which is consistent with the previous research FMT is used to clarify the influence of gut microbiota on the effects of theabrownin on NAFLD[1]. The observed improvements in lipid profiles and insulin resistance following FMT further highlight the potential of targeting the microbiota for the treatment of NAFLD. Collectively, the observed changes in gut microbiota composition and function suggest that CRA may exert its therapeutic effects on NAFLD through microbiota-dependent mechanisms, highlighting the importance of the gut-liver axis in disease pathophysiology and treatment changes in gut microbiota composition.

The analysis of CRA's impact on SCFAs and its subsequent effect on NAFLD via the gut-liver axis provides valuable insights into possible treatment strategies. Our findings indicate that CRA significantly alters the SCFA profile in both fecal and liver tissues, suggesting a direct influence on gut microbiota metabolism. Specifically, the elevation of butyrate levels in the CRA-treated groups corresponds with previous research highlighting butyrate's exerting anti-inflammatory effects to promote gut barrier integrity[35]. This modulation of SCFAs likely contributes to the observed improvements in liver health and overall metabolic status, as SCFAs are known to influence liver function through the gut-liver axis[41]. The consistency between fecal and liver SCFA profiles further supports the hypothesis that CRA exerts its therapeutic effects via altering the gut microbiota and its metabolites, which in turn affect liver health. This highlights the importance of the gut-liver axis in the pathophysiology of NAFLD and indicates that CRA may be a promising therapeutic agent for targeting this axis.

The transcriptomic analysis of liver tissue provides compelling evidence for the anti-NAFLD effects of CRA, revealing significant changes in gene expression profiles. Specifically, the gene expression pattern of the CRA treated group corresponded to that of the control group, suggesting a normalization of liver function at the molecular level. This convergence indicates that CRA may restore the liver's gene expression to a healthier state, mitigating the dysregulation associated with NAFLD. Enrichment study of DEGs with KEGG and GO databases highlighted key biological processes, such as phagosome activation and cytokine-cytokine receptor interaction. These processes are crucial for immune regulation and inflammation control. For instance, phagosome activation is essential for the clearance of pathogens and damaged cells, while cytokine-cytokine receptor interactions play a vital role in modulating immune responses[42]. The observed changes in these pathways suggest that CRA may exert its therapeutic effects by modulating immune-related processes, particularly those involved in cytokine production and phagocytosis. A particularly noteworthy pathway in this context is the cGAS-STING pathway, that's pivotal to immunological signaling and inflammation[41, 42]. The pathway detects cytosolic DNA from pathogens or damaged cells, resulting in the synthesis of interferons and pro-inflammatory cytokines[43]. The downregulation of key proteins in this pathway, such as NLRP3, cGAS, and IL-1β, in CRA-treated mice indicates that CRA may mitigate hepatitis by suppressing the pathway. This suppression likely reduces the secretion of inflammatory mediators and prevents pyroptosis, protecting liver cells from damage[44]. Collectively, these data highlight the intriguing possibility of CRA as a treatment agent for NAFLD, by modulating immune regulatory processes and reducing inflammation.

The cellular-level investigation of 'SCFAs' effects on NAFLD using HepG2 cells further supports the therapeutic potential of CRA. The observed enhancement of cell viability and reduction of TG and TC levels following SCFA treatment indicate that SCFAs, potentially regulated by CRA, can directly improve liver cell health. This aligns with prior research that SCFAs can modulate lipid metabolism and reduce inflammation[45]. The substantial reduction in inflammatory indicators, like NLRP3, cGAS, and IL-1β, in SCFA-treated cells suggests that SCFAs may suppress the cGAS-STING pathway, hence decreasing inflammation and protecting

liver cells from damage. The application for STING protein agonist DMXAA to suppress the inhibitory effects of SCFAs on principal proteins that participate in the cGAS-STING signaling pathway further confirms the dependence of SCFAs' anti-NAFLD effects on this pathway. This finding highlights the specificity of SCFAs' interaction with the STING-mediated pathway and suggests that SCFAs may exert their therapeutic effects by binding to specific receptors or components related to the STING protein[46]. Collectively, these results provide a comprehensive understanding of the therapeutic mechanisms of CRA in NAFLD, highlighting its potential as a microbiome-modulating agent that can improve liver health by modulating SCFA profiles and inhibiting inflammatory pathways, with the gut-liver axis implicated in this process[47, 48]. Future research should focus on elucidating the specific interactions between SCFAs and the STING protein, and exploring the prolonged consequences of CRA on gut microbiota and liver health. This will help to further clarify the mechanisms underlying CRA's therapeutic effects and its potential as a novel treatment for NAFLD.

5. Conclusion

This study demonstrated that CRA ameliorates HFD-induced liver inflammation and mitigates associated gains in body, liver and white adipose tissue weight. Its underlying mechanism appears to involve modulation of the gut–liver axis. This was evidenced by an improved gut microbial composition, enhanced gut barrier integrity, and a significant shift in specific populations: CRA advocated for the proliferation of advantageous, short-chain fatty acid-producing microorganisms (e.g., *Bacteroides* and *Prevotellaceae_UCG-001*) while suppressing bacteria often associated with detrimental health outcomes (e.g., *Lachnoclostridium, Ileibacterium*, and *Colidextribacter*). Consequently, increased SCFAs levels in substances from the intestines are conveyed to the liver by enterohepatic circulation. SCFAs inhibit mitophagy and reduce mtDNA release, thereby inhibiting cGAS-STING pathway activation, resulting in reduced IL-1β levels and an alleviation of inflammatory liver damage (Fig. 11). Taken together, these findings suggest that CRA has significant potential as a dietary source or a dietary supplement, potentially functioning as a prebiotic, for the prevention and management of NAFLD.

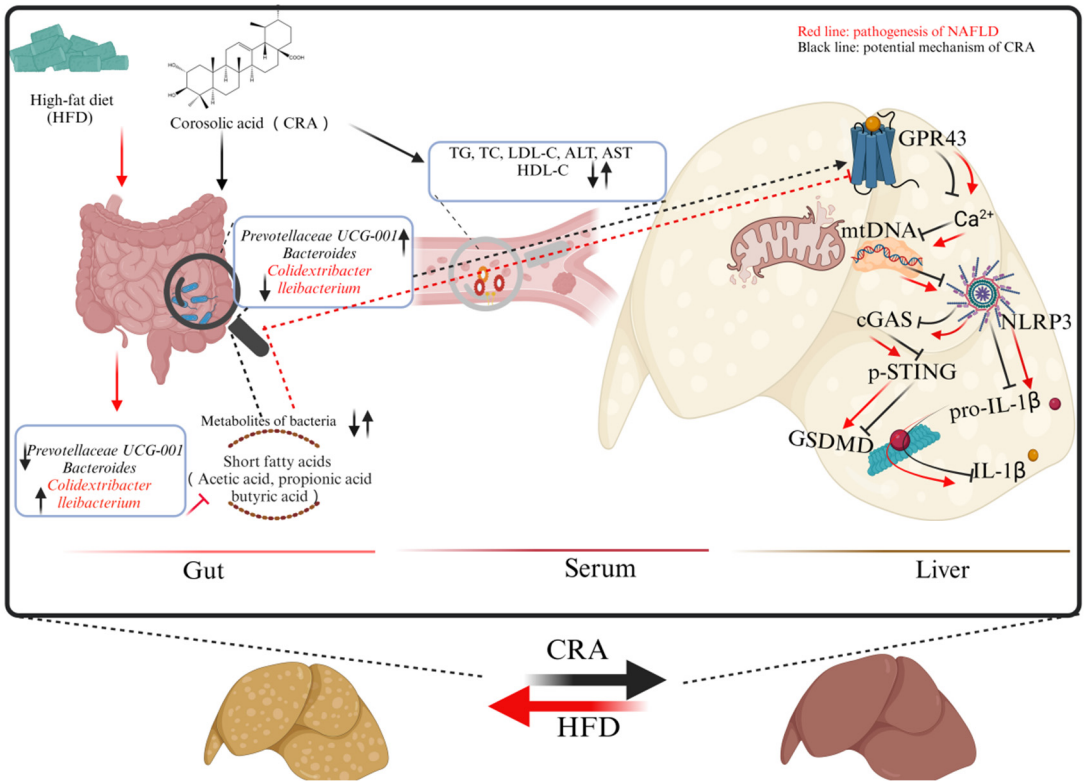


Fig. 11. Figure abstract.

Funding

Funding for this study was supplied by the Guangzhou Science and Technology Program (Grant No. 2023B03J1382), the Nansha Science and Technology Program (Grant No. 2022ZD004), and the Guangdong Basic and Applied Basic Research Foundation (Grant No. 2024A1515011747).

Ethics and animal study

All rodent studies were carried out at the Laboratory Animal Center of Guangzhou University of Chinese Medicine. The mice were sourced from Guangdong Medical Laboratory Animal Center (Foshan, China; SCXK 2022-0002) and underwent a seven-day acclimatization period in the animal breeding facility. The animal-related experiments strictly adhered to the guidelines and regulations set forth by the Institutional Animal Care and Use Committee of Guangzhou University of Chinese Medicine (ZYD-2023-231 & ZYD-2023-261). Every effort was made to reduce animal distress to the greatest extent possible.

Declaration of Competing Interest

The authors declare no financial conflicts or personal relationships that might influence this paper's work.

References

[1] H. Li, S. Huang, D. Zhou, et al., Theabrownin inhibits obesity and non-alcoholic fatty liver disease in mice via serotonin-related signaling pathways and gut-liver axis, J. Adv. Res. 52 (2023) 59-72. https://doi.org/10.1016/j.jare.2023.01.008.

[2] M. Kjaergaard, K.P. Lindvig, K.H. Thorhauge, et al., Using the ELF test, FIB-4 and NAFLD fibrosis score to screen the population for liver disease, J. Hepatol. 79 (2023) 277-286. https://doi.org/10.1016/j.jhep.2023.04.002.

[3] S. Yang, Z. Wei, J. Luo, et al., Integrated bioinformatics and multiomics reveal Liupao tea extract alleviating NAFLD via regulating hepatic lipid metabolism and gut microbiota, Phytomedicine. 132 (2024) 155834. https://doi.org/10.1016/j.phymed.2024.155834.

[4] Y, Lei, L, Tang, Q, Chen, et al., Disulfiram ameliorates nonalcoholic steatohepatitis by modulating the gut microbiota and bile acid metabolism, Nat. Commun. 13 (2022) 6862. https://doi.org/10.1038/s41467-022-34671-1.

[5] J. Behary, N. Amorim, X. Jiang, et al., Gut microbiota impact on the peripheral immune response in non-alcoholic fatty liver disease related hepatocellular carcinoma, Nat. Commun. 12 (2021) 187. https://doi.org/10.1038/s41467-020-20422-7.

[6] X. Zhang, O.O. Coker, E.S. Chu, et al. Dietary cholesterol drives fatty liver-associated liver cancer by modulating gut microbiota and metabolites, Gut. 70 (2021) 761-774. https://doi.org/10.1136/gutjnl-2019-319664.

[7] Y. Cheng, H. Qiu, X. Liu, et al., Chrysin alleviate obesity in mice by regulating gut microbiota and TLR4/JNK signaling pathway, Food Sci. Hum. Well. 2025, https://doi.org/10.26599/FSHW.2025.9250598.

[8] S.J. Yoon, J. Yu, B. Min, et al., *Bifidobacterium*-derived short-chain fatty acids and indole compounds attenuate nonalcoholic fatty liver disease by modulating gut-liver axis, Front. Microbiol. 14 (2023) 1129904. https://doi.org/10.3389/fmicb.2023.1129904.

[9] D. Stols-Gonçalves, A.L. Mak, M.S. Madsen, et al., Faecal microbiota transplantation affects liver DNA methylation in non-alcoholic fatty liver disease: a multi-omics approach, Gut Microbes. 15 (2023) 2223330. https://doi.org/10.1080/19490976.2023.2223330.

[10] R. Ding, H. Li, Y. Liu, et al., Activating cGAS-STING axis contributes to neuroinflammation in CVST mouse model and induces inflammasome activation and microglia pyroptosis, J. Neuroinflammation. 19 (2022) 137. https://doi.org/10.1186/s12974-022-02511-0.

[11] G. Wang, J. Liu, Y. Zhang, et al., Ginsenoside Rg3 enriches SCFA-producing commensal bacteria to confer protection against enteric viral infection via the cGAS-STING-type I IFN axis, ISME. J. 17 (2023) 2426-2440. https://doi.org/10.1038/s41396-023-01541-7.

[12] A. Caligiani, G. Malavasi, G. Palla, et al., A simple GC-MS method for the screening of betulinic, corosolic, maslinic, oleanolic and ursolic acid contents in commercial botanicals used as food supplement ingredients, Food Chem. 136 (2013) 735-741. https://doi.org/10.1016/j.foodchem.2012.08.011.

[13] G. Liu, Z. Cui, X. Gao, et al., Corosolic acid ameliorates non-alcoholic steatohepatitis induced by high-fat diet and carbon tetrachloride by regulating TGF-β1/Smad2, NF-κB, and AMPK signaling pathways, Phytother. Res. 35 (2021) 5214-5226. https://doi.org/10.1002/ptr.7195.

[14] X. Han, W. Zhao, Q. Zhou, et al., Procyanidins from hawthorn (Crataegus pinnatifida) alleviate lipid metabolism disorder via inhibiting insulin resistance and oxidative stress, normalizing the gut microbiota structure and intestinal barrier, and further suppressing hepatic inflammation and lipid accumulation, Food Funct. 13 (2022) 7901-7917. https://doi.org/10.1039/d2fo00836j.

[15] P. Hao, X. Yang, W. Yin, et al., A study on the treatment effects of Crataegus pinnatifida polysaccharide on non-alcoholic fatty liver in mice by modulating gut microbiota, Front. Vet. Sci. 11 (2024) 1383801. https://doi.org/10.3389/fvets.2024.1383801.

[16] J. Yang, J. Leng, J. Li, et al., Corosolic acid inhibits adipose tissue inflammation and ameliorates insulin resistance via AMPK activation in high-fat fed mice, Phytomedicine. 23 (2016) 181-190. https://doi.org/10.1016/j.phymed.2015.12.018.

[17] H. Xia, X. Zhu, X. Zhang, et al., Alpha-naphthoflavone attenuates non-alcoholic fatty liver disease in oleic acid-treated HepG2 hepatocytes and in high fat diet-fed mice, Biomed. Pharmacother. 118 (2019) 109287. https://doi.org/10.1016/j.biopha.2019.109287.

[18] X. Li, W. Zhao, M. Xiao, et al., Penthorum chinense Pursh. extract attenuates non-alcholic fatty liver disease by regulating gut microbiota and bile acid metabolism in mice, J. Ethnopharmacol. 294 (2022) 115333. https://doi.org/10.1016/j.jep.2022.115333.

[19] Q. Liang, Y. Zheng, F. Meng, et al., Palmitoleic acid on top of HFD ameliorates insulin resistance independent of diacylglycerols and alters gut microbiota in C57BL/6J mice, Food Sci. Hum. Well. 13 (2024) 856-868. https://doi.org/10.26599/FSHW.2022.9250073.

[20] R. Molani-Gol, A. Dehghani, M. Rafraf, Effects of curcumin/turmeric supplementation on the liver enzymes, lipid profiles, glycemic index, and anthropometric indices in non-alcoholic fatty liver patients: An umbrella meta-analysis, Phytother. Res. 38 (2024) 539-555. https://doi.org/10.1002/ptr.8051.

[21] J. Zhong, X. He, X. Gao, et al., Hyodeoxycholic acid ameliorates nonalcoholic fatty liver disease by inhibiting RAN-mediated PPARα nucleus-cytoplasm shuttling, Nat. Commun. 14 (2023) 5451. https://doi.org/10.1038/s41467-023-41061-8.

[22] Y. Du, C. He, Y. An, et al., The Role of short chain fatty acids in inflammation and body health, Int. J. Mol. Sci. 25 (2024) 7379. https://doi.org/10.3390/ijms25137379.

[23] D.H. Lee, M.T. Kim, J.H. Han, GPR41 and GPR43: From development to metabolic regulation, Biomed. Pharmacother. 175 (2024) 116735. https://doi.org/10.1016/j.biopha.2024.116735.

[24] Z. Zheng, N. Sun, J. Yang, et al., Sea cucumber gut tetrapeptide ameliorates alcoholic gastric damage via restoring mitochondrial dynamics, Food Sci. Hum. Well. 14 (2025) 9250183. https://doi.org/10.26599/FSHW.2024.9250183.

[25] J. Lin, H. Liu, Y. Sun, et al., Arabinoxylan alleviates obesity by regulating gut microbiota and bile acid metabolism, J. Agric. Food Chem. 72 (2024) 23295-23305. https://doi.org/10.1021/acs.jafc.4c06392.

[26] D.S. Jang, G.Y. Lee, J. Kim, et al., A new pancreatic lipase inhibitor isolated from the roots of Actinidia arguta, Arch. Pharm. Res. 31 (2008) 666-670. https://doi.org/10.1007/s12272-001-1210-9.

[27] Y. Peng, N. Li, F. Tang, et al., Corosolic acid sensitizes ferroptosis by upregulating HERPUD1 in liver cancer cells, Cell Death Discov. 8 (2022) 376. https://doi.org/10.1038/s41420-022-01169-0.

[28] C. Ren, M. Gao, N. Li, et al., Identification and mechanism elucidation of medicative diet for food therapy XQCSY in NAFLD prevention: an integrative in silico study. Food & Medicine Homology. 1 (2024) 9420015. https://doi.org/10.26599/FMH.2024.9420015

[29] A. Monga Kravetz, T. Testerman, B. Galuppo, et al., Effect of gut microbiota and PNPLA3 rs738409 variant on nonalcoholic fatty liver disease (NAFLD) in obese youth, J. Clin. Endocrinol. Metab. 105 (2020) e3575-e3585. https://doi.org/10.1210/clinem/dgaa382.

[30] L. Tong, S. Zhang, Q. Liu, et al., Milk-derived extracellular vesicles protect intestinal barrier integrity in the gut-liver axis, Sci. Adv. 9 (2023) eade5041. https://doi.org/10.1126/sciadv.ade5041.

[31] C. Jin, R.A. Flavell, Innate sensors of pathogen and stress: linking inflammation to obesity, J. Allergy Clin. Immunol. 132 (2013) 287-294. https://doi.org/10.1016/j.jaci.2013.06.022.

[32] A. Agodi, C. Ojeda-Granados, A. Maugeri, et al., Changes in gut microbial composition and DNA Methylation in Obese Patients with NAFLD after bariatric surgery, Int. J. Mol. Sci. 25 (2024) 11510. https://doi.org/10.3390/ijms252111510.

[33] W. Zhang, W. Cheng, J. Li, et al., New aspects characterizing non-obese NAFLD by the analysis of the intestinal flora and metabolites using a mouse model, mSystems. 9 (2024) e0102723. https://doi.org/10.1128/msystems.01027-23.

[34] K. Bauer Estrada, N. Conde-Martínez, A. Acosta-González, et al., Synbiotics of encapsulated *Limosilactobacillus fermentum K73* promotes in vitro favorable gut microbiota shifts and enhances short-chain fatty acid production in fecal samples of children with autism spectrum disorder, Food Res. Int. 209 (2025) 116227. https://doi.org/10.1016/j.foodres.2025.116227.

[35] Q. Wang, J. Liang, Q. Zou, et al., Tryptophan metabolism-regulating probiotics alleviate hyperuricemia by protecting the gut barrier integrity and enhancing colonic uric acid excretion, J. Agric. Food Chem. 72 (2024) 26746-26761. https://doi.org/10.1021/acs.jafc.4c07716.

[36] A.L. Jaffe, J.F. Banfield, Candidate phyla radiation bacteria, Curr. Biol. 34 (2024) R80-R81. https://doi.org/10.1016/j.cub.2023.12.024.

[37] L. Yang, Y. Wang, Z. Li, et al., Brain targeted peptide-functionalized chitosan nanoparticles for resveratrol delivery: Impact on insulin resistance and gut microbiota in obesity-related Alzheimer's disease, Carbohydr. Polym. 310 (2023) 120714. https://doi.org/10.1016/j.carbpol.2023.120714.

[38] X. Song, J. Sun, Y. Yue, et al., Microbiota-derived succinic acid mediates attenuating effect of dietary tomato juice supplementation on steatohepatitis through enhancing intestinal barrier, Food Res. Int. 196 (2024) 115123. https://doi.org/10.1016/j.foodres.2024.115123.

[39] J. Lin, H. Liu, Y. Sun, et al., Arabinoxylan alleviates obesity by regulating gut microbiota and bile acid metabolism. J. Agric. Food Chem. 72 (2024) 23295-23305. https://doi: 10.1021/acs.jafc.4c06392.

[40] Y. Liu, S. Chen, Y., Y. Chen, et al., Polysaccharides extracted from common buckwheat (Fagopyrum esculentum) attenuate cognitive impairment via suppressing RAGE/p38/NF-κB signaling and dysbiosis in AlCl3-treated rats. Int. J. Biol. Macromol. 276 (2024), 133898. https://doi.org/10.1016/j.ijbiomac.2024.133898

[41] Y. Yin, A. Sichler, J. Ecker, et al., Gut microbiota promote liver regeneration through hepatic membrane phospholipid biosynthesis, J. Hepatol. 78 (2023) 820-835. https://doi.org/10.1016/j.jhep.2022.12.028.

[42] X. Gui, H. Yang, T. Li, et al., Autophagy induction via STING trafficking is a primordial function of the cGAS pathway, Nature. 567 (2019) 262-266. https://doi.org/10.1038/s41586-019-1006-9.

[43] C. Ding, Z. Song, A. Shen, et al., Small molecules targeting the innate immune cGAS–STING–TBK1 signaling pathway, Acta. Pharm. Sin. B. 10 (2020) 2272-2298. https://doi.org/10.1016/j.apsb.2020.03.001.

[44] S. Gaul, A. Leszczynska, F. Alegre, et al., Hepatocyte pyroptosis and release of inflammasome particles induce stellate cell activation and liver fibrosis, J. Hepatol. 74 (2021) 156-167. https://doi.org/10.1016/j.jhep.2020.07.041.

[45] K. Ye, Y. Zhao, W. Huang, et al., Sodium butyrate improves renal injury in diabetic nephropathy through AMPK/SIRT1/PGC-1α signaling pathway, Sci. Rep. 14 (2024) 17867. https://doi.org/10.1038/s41598-024-68227-8.

[46] X. Luo, H. Li, L. Ma, et al., Expression of STING is increased in liver tissues from patients with NAFLD and promotes macrophage-mediated hepatic inflammation and fibrosis in mice, Gastroenterology. 155 (2018) 1971-1984.e4. https://doi.org/10.1053/j.gastro.2018.09.010.

[47] L. Cao, Y. Wu, K. Liu, et al., Cornus officinalis vinegar alters the gut microbiota, regulating lipid droplet changes in nonalcoholic fatty liver disease model mice. Food & Medicine Homology. 1 (2024) 9420002. https://doi.org/10.26599/FMH.2024.9420002.

[48] B. Zhu, J. Li, Q. Zhang, Refining the gut-microbiome axis: A triad of metabolites, targeted microbial delivery, and AI-assisted profiling for precision medicine-food intervention. Food & Medicine Homology. 2025, https://doi.org/10.26599/FMH.2025.9420118.